RSC Advances

PAPER

View Article Online
View Journal | View Issue

Cite this: *RSC Adv.*, 2025, **15**, 25291

Piperidine and valproic acid hybrid compound (F2S4-*p*-VPA) outperforms methotrexate as anti-proliferative and cells migration inhibition†

Martha Cecilia Rosales Hernández, ‡*[a] Raúl Horacio Camarillo López,‡[a] Marycruz Olvera-Valdez,[b] Leticia Guadalupe Fragoso Morales,[ac] Itzia Irene Padilla Martínez,[d] Mónica Adriana Torres Ramos,[e] Marycarmen Godínez Victoria,[f] Raúl Flores Mejía[g] and José Correa Basurto *[c]

Glioblastoma and triple-negative breast cancer (TNBC) pose significant challenges in treatment due to their invasive nature and propensity for metastasis. Methotrexate (**MTX**) is a common chemotherapeutic agent; however, it has limited efficacy owing to its low aqueous solubility and cytostatic rather than cytotoxic effects. Valproic acid (**VPA**) has been used as chemotherapeutic agent, but with low potency. In this study, two novel **VPA** derivatives (**F2S4-*p*-VPA** and **F3S4-*m*-VPA**) were designed, chemically synthesized, and evaluated *in vitro*. These compounds contain tertiary amines as pharmacophore groups reminiscent of methotrexate. Cytotoxicity, migration, assays were conducted on glioblastoma (LN-18, U373) and breast cancer (MDA-MB-231) cell lines, using fibroblast (3T3-L1; non-cancer cells) as a control. Apoptosis (LN-18 and MDA-MB-231), cell cycle arrest and Bax and Bcl2 assays were carried out on LN-18 cells. Physicochemical properties of the compounds were assessed using *in silico* predictions. Results showed that **F2S4-*p*-VPA** exhibited better cytotoxicity than **F3S4-*m*-VPA** on both LN-18 (IC_{50} = 112 μM) and MDA-MB-231 (IC_{50} = 142 μM) cell lines, while demonstrating reduced cytotoxicity in 3T3-L1 cells. **F2S4-*p*-VPA** inhibited cell migration, outperforming **MTX**. Moreover, **F2S4-*p*-VPA** induced the highest rate of apoptosis in LN-18 cell, and produce the cell cycle arrest in the S and G2/M phase, showing a Bax/Bak-independent propapoptotic effect suggesting other mechanisms of cell death. Also, these novel compounds possess superior physicochemical properties to **MTX** and **VPA**. These results suggest that **F2S4-*p*-VPA** warrants further investigation *in vivo* and may serve as structural scaffold for the development of novel compounds for the treatment of these aggressive cancers.

Received 25th February 2025
Accepted 3rd July 2025

DOI: 10.1039/d5ra01365h

rsc.li/rsc-advances

1. Introduction

According to the World Health Organization, cancer is a leading cause of death globally, accounting for nearly 10 million deaths in 2020, or nearly one in six deaths. Furthermore, cancer is the leading cause of death before the age of 70 in 112 out of 183 countries.[1] GLOBOCAN estimate 28.4 million new cancer cases to occur in 2040 year.[2] Cancer has become a global health problem brain cancer with 308 102 new cases in 2020, though

[a]*Laboratorio de Biofísica y Biocatálisis, Sección de Estudios de Posgrado e Investigación, Escuela Superior de Medicina, Instituto Politécnico Nacional, Plan de San Luis y Díaz Mirón s/n, Casco de Santo Tomás, Distrito Federal, 11340, Mexico. E-mail: marcrh2002@yahoo.com.mx*

[b]*Laboratorio Nanomateriales Sustentables, Sección de Estudios de Posgrado e Investigación – Escuela Superior de Ingeniería Química e Industrias Extractivas, Instituto Politécnico Nacional, Av. Instituto Politécnico Nacional S/N, Unidad Profesional Adolfo López Mateos, CP 07708, CDMX, Mexico*

[c]*Laboratorio de Diseño y Desarrollo de Nuevos Fármacos e Innovación Biotecnológica, Sección de Estudios de Posgrado e Investigación, Escuela Superior de Medicina, Instituto Politécnico Nacional, Plan de San Luis y Díaz Mirón s/n, Casco de Santo Tomás, Distrito Federal, 11340, Mexico. E-mail: corrjose@gmail.com*

[d]*Laboratorio de Química Supramolecular y Nanociencias, Unidad Profesional Interdisciplinaria de Biotecnología del Instituto Politécnico Nacional, Av. Acueducto s/n Barrio la Laguna Ticomán, CDMX, 07340, Mexico*

[e]*Dirección de Investigación, Instituto Nacional de Neurología y Neurocirugía Manuel Velasco Suárez, Ciudad de México and Centro de Investigación sobre el Envejecimiento, CINVESTAV sede sur., Av. Insurgentes Sur, 3877 Col. La Fama, 14269. Tlalpan, Mexico*

[f]*Laboratorio de Citometría de Flujo, Sección de Estudios de Posgrado e Investigación, Escuela Superior de Medicina, Instituto Politécnico Nacional, CDMX, Mexico*

[g]*Laboratorio de Inflamación y Obesidad, Escuela Superior de Medicina, Instituto Politécnico Nacional, Plan de San Luis y Díaz Mirón, Ciudad de México, 11340, Mexico*

† Electronic supplementary information (ESI) available: Appendix A. Supplementary data. See DOI: https://doi.org/10.1039/d5ra01365h

‡ These authors participated equal.

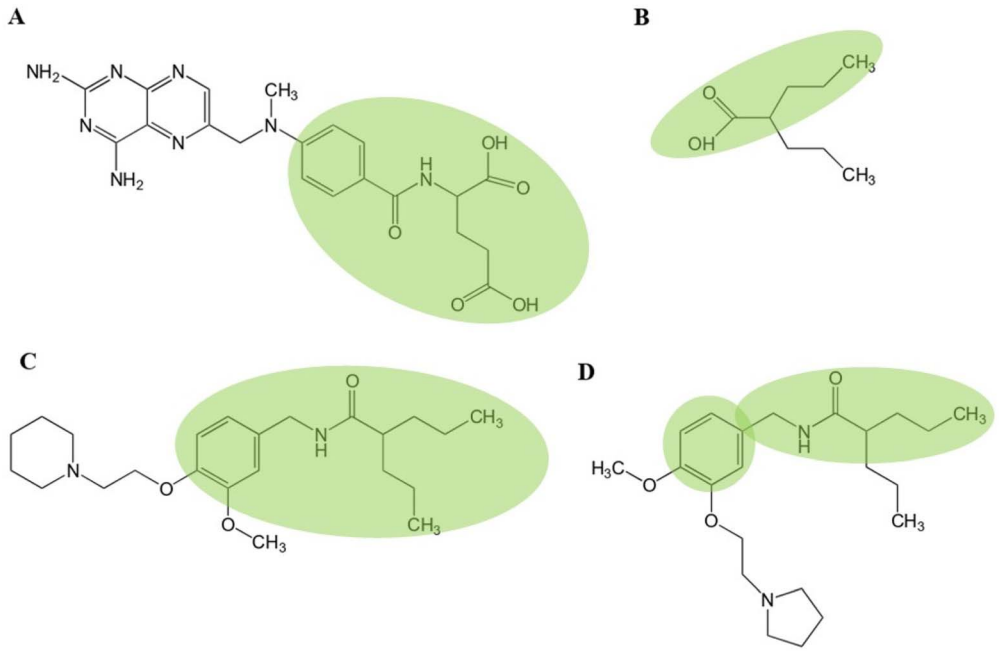

Fig. 1 Chemical structures of (A) methotrexate, (B) valproic acid, (C) F2S4-*p*-VPA, (D) F3S4-*m*-VPA indicating in green the chemical relationship between the structures.

with fewer deaths compared to breast cancer (BC)[3] which is the most common, accounting for 2.26 million new cases.[1]

Regarding brain cancer in Mexico, it ranks as the second leading cause of death in the pediatric population (below 15 years) encompassing the malignant tumors of the meninges, encephalon and other central nervous system tumors (18% in males and 15% in females).[4] Specifically, glioblastoma emerges as the most common primary intracranial tumor.[5] Glioblastoma multiforme (GBM) is known for its aggressiveness and lethality, characterized by rapid proliferation and resistance due invasive infiltration into surrounding brain tissue.[6,7] Both pediatric and adult population experience high mortality and morbidity rates, with an incidence of 3.19 cases per 100 000 individuals.[8]

BC has been the most common cancer among women since 2006 (ref. 9) and is one of the main reasons of morbidity and mortality in Mexico, accounting for 15.3% of new cases in 2020.[3] Ductal adenocarcinoma is the most frequent type of BC in Mexican women.[10] However, triple-negative breast cancer (TNBC), characterized by negative expression of estrogenic receptor (ER) and progesterone receptor (PR), and absence of amplification of the human epidermal growth factor-2 (HER2) gene, is the more prevalent in women under 40.[11]

These cancer types, GBM and TNBC undergo significant metastatic processes within a conducive environment characterized by factors such as hypoxia, extracellular matrix stiffness and nutrient deprivation, facilitating cell proliferation, migration, and invasion into secondary sites.[12,13] Inflammation can further exacerbate chromosomal instability and promote cancer metastasis.[14] Nearly 25% of the solid tumours arise from chronic inflammation, recognized as a hallmark of cancer. Elevated levels of inflammatory cells correlates with increased metastasis, often accompanied by the presence of cytokines, such as interleukin (IL)-6, tumor necrosis factor (TNF)-α, IL-1 and interferon (IFN)-γ and chemokines such as CXCL12, CXCL14 and CCL7.[15] It has been reported that lipopolysaccharide (LPS) can induce migration and invasion in various cancer cells through inflammation activation, as in breast cancer.[16–18] Additionally, *in vitro* studies have demonstrated the challenging nature of treating GBM and TNBC cells due to their high aggressiveness and propensity for invasion and migration, particularly when stimulated with TNF-α, phorbol 12-myristate 13-acetate (PMA) or LPS.[7,17]

Currently, there are different chemotherapy options to treat cancer as methotrexate (**MTX**).[19] **MTX** is used to treat BC, including in patients whose cancer has metastasized. Formerly known as amethopterin, it is an antifolate that acts as both an anti-neoplastic agent and a suppressor of immune system.[20] **MTX** has been combined with other anticancer drugs used to treat BC, such as mitomycin C, cyclophosphamide, and 5-fluorouracil or in combination with vitamin C.[21] Additionally, **MTX** has been evaluated in glioma cells, decreasing cell viability in treatment for 48 h.[22] However, to evaluate **MTX** in clinical trials of glioblastoma, high doses are necessary to cross the blood brain barrier (BBB).[23]

On the other hand, valproic acid (2-propylpentanoic acid; **VPA**) has been used either directly or synergistically as an anti-glioma agent either *in vitro* or *in vivo* studies.[24,25] **VPA** is a short-chain fatty acid, a member of the group of histone deacetylase inhibitors (HDACIs) that has the capacity to inhibit cancer cell proliferation by modulating multiple intracellular signaling pathways and it is an agent used to limit proliferation of tumor cells.[26,27] It has been demonstrated that **VPA** exhibits anticancer

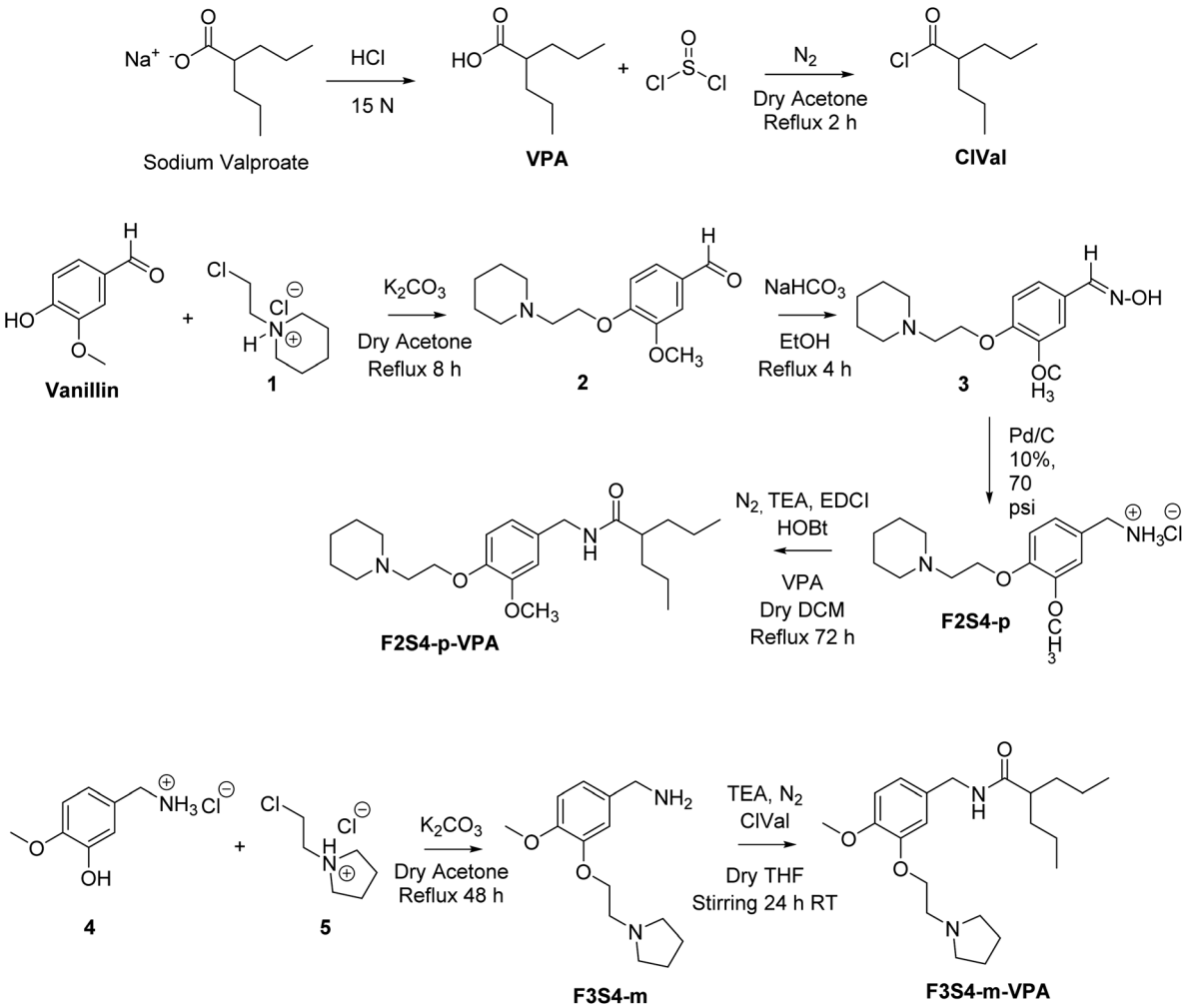

Scheme 1 Chemical synthesis of F2S4-*p*-VPA and F3S4-*m*-VPA.

activity in a variety of human cancers, including BC and glioma principally inducing a cellular differentiation, growth arrest, and apoptosis.[28] Several studies have revealed that **VPA** sensitizes GBM cells to chemotherapy and radiotherapy by increasing cell apoptosis and cell cycle arrest, and activating proapoptotic signaling.[25,29]

VPA derivatives have been explored for their anticancer properties, particularly against breast cancer. 2-Hexyl-4-pentynoic acid (HPTA), for example, proved highly effective: at just 15 μM, has the same effects of 500 μM **VPA** in inhibiting breast cancer cell growth and sensitizing MCF7 cells to hydroxyurea.[30,31] HPTA also improved breast tumor radiosensitivity in rats by inhibiting Rad51.[32] Additionally, *N*-(2′-hydroxyphenyl)-2-propylpentanamide (OH–VPA), a histone deacetylase inhibitor, was shown to induce nuclear HMGB1 release and alter ROS levels in HeLa cells.[33] While VPA itself has shown potential in sensitizing glioblastoma to radiation therapy[34,35] it's important to note that some reports indicate a limited effect of **VPA** on clinical outcomes for glioblastoma patients.[36] Other research by M. Farroq *et al.* includes the synthesis and biological evaluation of various Schiff base series of valproyl derivatives for anticancer use.[37]

Due to high heterogeneity of GBM and TNBC characterized by their aggressiveness, developing new therapies to treat them could be a priority. The goal of this research is to evaluate new **VPA** derivatives (**F2S4-*p*-VPA** and **F3S4-*m*-VPA**) comparing them with **MTX** which is used as pharmacological therapy to treat TNBC and GBM cells (Fig. 1). While **VPA** has shown antiproliferative effects on cancer cells, it is not widely used due to its low potency and cytotoxic. However, it serves as scaffold to add chemical pharmacophores present in **MTX** when linked to a tertiary amine yielding **F2S4-*p*-VPA** and **F3S4-*m*-VPA**; the chemical synthesis is presented in Scheme 1. Therefore, their cytotoxic activity and their ability to inhibit cell migration were tested on human malignant glioma (LN-18), human glioblastoma astrocytoma (U373), invasive ductal carcinoma (MDA-MB-231), a tumor with positive expression of epidermal growth factor (EGF) and transforming growth factor alpha (TGF-α); and fibroblast cell line (3T3-L1) non cancer cells used the later as a control. Also, the apoptosis and the expression of anti-apoptotic and apoptotic proteins and cell cycle assays with propidium iodide, were determinate by flow cytometry. The results indicated that **F2S4-*p*-VPA** exhibits better cytotoxic and cytostatic effects compared to **MTX**. Hence, it serves as an

alternative for treating these aggressive cell types or be employed as a core for designing new compounds.

2. Materials and methods

2.1 Chemical synthesis

All chemical reactants and starting materials purchased from Sigma-Aldrich were directly used without further purification. All solvents were distilled prior to use. The acetone was dried by adding molecular sieves 3 Å, swirling the mixture and allowing it to sit overnight before decanting the acetone off the drying agent.

Mass spectra studies were executed by staff of Escuela Superior de Medicina using a Q-TOF (model 6545) with an ESI (model G1959A) Agilent. Thin layer chromatography (TLC) was performed using commercially available pre-coated plates (TLC silica gel 60 F_{254}). Column chromatography was carried out using Merck silica gel 60 (0.063–0.100 mm).

The synthesized compounds were characterized through ^{1}H and ^{13}C NMR spectroscopy. All spectra were recorded on a Varian 300 MHz spectrometer. Samples of compounds were dissolved in the indicated deuterated solvent; chemical shifts (δ) were reported in ppm downfield to tetramethylsilane. Coupling constants (J) are reported in Hertz and rounded to 0.1 Hz. Splitting patterns are abbreviated as follows: singlet (s), doublet (d), triplet (t), quintet (q), multiplet (m), broad (br) or a combination of these.

The synthesis of valproic chloride (ClVal), **F2S4-*p*-VPA** and **F3S4-*m*-VPA** is depicted in Scheme 1. The synthetic route for **F2S4-*p*** and **F3S4-*m*** compounds has been previously reported by our group.[38] Briefly, the synthesis of compound **F2S4-*p*** followed a different approach to obtain the amine group in *para* position relative to the alkoxy group; for this purpose, the Williamson ether synthesis was performed employing 4-hydroxy-3-methoxybenzaldehyde (vanillin) and 1-(2-chloroethyl)piperidine hydrochloride (**1**) as the starting materials to lead the compound (**2**). The next step required the formation of the appropriate oxime (**3**) which ultimately was further reduced to the desired amine employing a catalytic hydrogenation procedure. Compound **F3S4-*m*** was obtained *via* the Williamson ether synthesis, in which a hydroxy-benzylamine derivative (**4**) reacted with 1-(2-chloroethyl) pyrrolidine hydrochloride (**5**) a primary alkyl halide *via* a nucleophilic substitution reaction. The functionalization of **F2S4-*p*** to yield **F2S4-*p*-VPA** involved an analogous acyl substitution reaction with valproic acid, facilitated by TEA, 1-ethyl-3-(3-dimethylaminopropyl)carbodiimide (EDCI), and 1-hydroxybenzotriazole (HOBt). This transformation was conducted under reflux conditions in anhydrous dichloromethane (DCM) for 72 hours, ensuring optimal coupling efficiency. The derivatization of **F3S4-*m*** to **F3S4-*m*-VPA** was accomplished *via* a nucleophilic acyl substitution, wherein **F3S4-*m*** reacted with ClVal in the presence of triethylamine (TEA) as a base, under anhydrous conditions in tetrahydrofuran (THF) and an inert nitrogen atmosphere, with continuous stirring at ambient temperature for 24 hours.

2.1.1 Synthesis of *N*-(3-methoxy-4-(2-(piperidin-1-yl)ethoxy) benzyl)-2-propylpentanamide (F2S4-*p*-VPA). To synthesize **F2S4-*p*-VPA**, it was first necessary to obtain the **VPA**, the valproic chloride and **F2S4-*p***.

2.1.1.1 Synthesis of 2-propylpentanoic acid (valproic acid). Sodium valproate (1.00 g, 6.9 mmol) was dissolved in distilled water (15 mL) in a 50 mL beaker. The pH was adjusted to 4.0 by dropwise addition of 15 N HCl. The resulting **VPA**, appearing as a colorless liquid, separated from the aqueous layer and remained on the surface. The **VPA** was then extracted with ethyl acetate (2 × 15 mL) employing a 100 mL separating funnel. The organic fraction was then washed with distilled water (2 × 20 mL), dried with anhydrous Na_2SO_4, and filtered to remove the solid Na_2SO_4. The solvent was then evaporated under reduced pressure (240 mbar, 60 °C) to obtain the **VPA** as a colorless liquid (1.8 mL), which was used without further purification.

2.1.1.2 Synthesis of valproic chloride (ClVal). **VPA** (1.8 mL) was placed into a 100 mL two-neck round-bottom flask containing a magnetic stirrer (10 mm long, 7 mm wide). Thionyl chloride (0.65 mL, 9.08 mmol) was then added dropwise to the flask. The mixture was then refluxed for 2 h in dry acetone using a cooling system (ECO 30®) and a heating mantle connected to a thermal cycler (Thermolyne 45500®) to reach 80 °C. The reaction was protected from moisture using a nitrogen-filled balloon. Residual $SOCl_2$ was removed with the aid of a Schlenk line. The resulting valproic chloride was stored at −20 °C under a nitrogen atmosphere to protect it from air until further use.

The synthesis of **F2S4-*p*** was performed according to procedures previously reported by our group[38] employing peptide synthesis methodologies as these conditions are normally gentle and provide high yields.

A mixture of **F2S4-*p*** (500 mg, 1.67 mmol), EDCI (320 mg, 1.7 mmol) and HOBt (260 mg, 1.7 mmol) was dissolved with dry dichloromethane (75 mL) into a 100 mL two-neck round-bottom flask containing a magnetic stirrer (10 mm long, 7 mm wide) under an N_2 atmosphere. Afterwards, **VPA** (235 μL, 1.8 mmol) and TEA (2.5 mL) were added to the mixture allowing the reaction to proceed 72 h under refluxing conditions. The reaction mixture was then extracted with pH-adjusted water (3 × 100 mL) to remove traces of **VPA** and remaining coupling reagents. The organic phase was dried with anhydrous sodium sulfate, and solvent was removed by reduced pressure. The obtained residue was purified by silica column chromatography employing a mixture of solvents, starting with hexane, and gradually transitioning to ethyl acetate as the sole solvent. Eventually, ethanol was added to achieve a 25% mixture of ethyl acetate and ethanol. The **F2S4-*p*-VPA** was obtained as pale-yellow powder (54% yield, 97% purity), mp 97 °C. IR (cm^{-1}): 3283 (N–H stretching), 1638 (C=O stretching), 1544 (aromatic C=C stretches), 1515 (in plane N–H companion bend), 1237 (C–N stretch), 707 (N–H wag out of plane).^{1}H-NMR (300 MHz, $CDCl_3$, ppm) 6.83 (m, 3H, H-1, H-3, H-6), 5.76 (br, 1H, NH), 4.40 (d, J = 5.66, 2H, $PhCH_2$), 4.15 (t, J = 6.44, 2H, H-7), 3.83 (s, 3H, OCH_3), 2.83 (t, J = 6.43, 2H, H-8), 2.54 (t, 4H, H-9), 2.05 (q, J = 4.68, 1H, H-12), 1.62 (t, J = 6.54, 4.11, 4H, H-10), 1.47–1.23 (m, 10H, H-11, H-13, H-14),0.89 (t, J = 6.96, 6H, H-15). ^{13}C NMR (75 MHz, $CDCl_3$, ppm) 175.9 (C=O), 149.7 (C-4),147.7 (C-3), 131.8 (C-6), 120.1 (C-1), 113.2 (C-2), 111.5 (C-5), 66.8 (C-7), 57.8 (C-8),

55.92 (OCH_3), 55.12 (C-9), 47.94 (C-12), 43.24 (Ph-CH_2), 35.4 (C-13), 25.9 (C-10), 24.2 (C-11), 21.0 (C-14), 14.3 (C-15). MS (ESI^+): *m*/*z* calculated for ($[C_{23}H_{38}N_2O_3]$ + $H)^+$: 391.2955, found 391.2958, calculated for ($[C_{23}H_{38}N_2O_3]$ + $Na)^+$: 413.2775 found 413.2677. All proton and carbon NMR, FTIR and mass spectra for **F2S4-*p*-VPA** are available for consultation in the ESI under Sections S1 to S4.†

2.1.2 Synthesis of *N*-(4-methoxy-3-(2-(pyrrolidin-1-yl) ethoxy)benzyl)-2-propylpentanamide (F3S4-*m*-VPA)

2.1.2.1 Synthesis of (4-methoxy-3-(2-(pyrrolidin-1-yl)ethoxy) phenyl) methanamine (F3S4-m). The synthesis of **F3S4-*m*** has been previously reported by our group.[38] The synthesis involves reacting 3-hydroxy-4-methoxybenzylamine hydrochloride with 1-(2-chloroethyl)pyrrolidine hydrochloride in the presence of K_2CO_3 in dry acetone under refluxing conditions for 48 h. The resulting viscous residue was purified by alumina gel column chromatography, yielding **F3S4-*m*** with a 75% yield and 96% purity.

2.1.2.2 Synthesis of F3S4-m-VPA. **F3S4-*m*** (1.31 g, 5.25 mmol) was placed into an ice-cooled 100 mL two-neck round-bottom flask containing a magnetic stirrer (10 mm long, 7 mm wide) under N_2 atmosphere. Triethylamine (TEA, 0.56 mL, 12.6 mmol) was then added to the flask followed by dropwise addition of a ClVal (0.9 mL, 6.3 mmol) previously diluted in THF (3 mL) corresponding to a 1.2 mol of ClVal per each mol of 3-hydroxy-4-methoxybenzylamine hydrochloride. The mixture remained under cooled stirring for 15 min. Afterwards, the mixture was stirred for 24 h under room temperature (rt). The heterogeneous mixture was vacuumed-filtered, the solid phase was washed with THF (10 mL). All liquid fractions were collected, and solvent was removed by reduced pressure (374 mbar, 60 °C) to finally obtain a thick dark brownish liquid.

For purification of **F3S4-*m*-VPA**, 100 mg of **F3S4-*m*-VPA** was diluted in distilled hexane (20 mL) under stirring conditions over 20 min. Thereafter, the mixture was chilled over 48 h at 4 °C leading the formation to a light brown-sand colour precipitate. The solid was then removed with the aid of vacuum filtration followed by removal of traces of solvent with a Schlenk line overnight.

F3S4-*m*-VPA was obtained as a light brown solid (556 mg, 55.6% yield, 96% purity). m. p. 94 °C. IR (cm^{-1}) 3290 (N–H stretching), 3082 (C–H stretch), 1635 (C=O stretching), 1517 (in plane N–H companion bend), 1553 (aromatic C=C stretches), 707 (N–H wag out of plane). ^{1}H NMR (300 MHz, $CDCl_3$, ppm); 6.83 (d, J = 1.12, 1H, H-3), 6.80 (s, 2H, H-1, H-6), 5.79 (br, NH), 4.37 (d, J = 5.64 2H, $PhCH_2$), 4.11 (t, J = 6.01, 2H, H-7), 3.83 (s, 3H, OCH_3), 2.95 (t, J = 6.15, 2H, H-8), 2.65 (t, J = 3.34, 8.66 4H, H-9), 2.07–1.96 (m, 1H, H-11), 1.80 (q, J = 14.86, 8.25, 4H, H-10), 1.69–1.32 (m, 4H, H-12), 1.32–1.14 (m, 4H, H-13), 0.87 (t, J = 7.12, 6.99, 6H, H-14). ^{13}C NMR (75 MHz, $CDCl_3$, ppm) δ 175.9 (C=O), 148.8 (C-4),148.4 (C-5), 131.3 (C-2), 120.5 (C-1), 113.0 (C-6), 111.6 (C-3), 67.5 (C-7), 56.0 (C-8), 54.8 (C-9), 54.5 (OCH_3), 47.9 (Ph-CH_2), 43.2(C-11), 35.40 (C-12), 25.5 (C-10), 21.0 (C-13), 14.3 (C-14). MS (ESI^+): *m*/*z* calculated for ($[C_{22}H_{36}N_2O_3]$ + $H)^+$: 377.2799, found: 377.2788. All proton and carbon NMR, FTIR and mass spectra for **F3S4-*m*-VPA** are available for consultation in the ESI under Sections S5 to S8.†

2.2 *In vitro* studies

2.2.1 Cell lines and culture. MDA-MB-231 was procured from ATTC (HTB-26). Glioblastoma cell lines (U373 and LN-18)[39] were generously provided by Dr. Monica Torres from Instituto Nacional de Neurología y Neurocirugía de Mexico (INNN)), and the fibroblast cell line (3T3-L1) non cancer cells was kindly provided by Dra. Ivonne Olivares Corichi (Instituto Politécnico Nacional, Escuela Superior de Medicina). 3T3-L1 cells were used without differentiation solely as a control for fibroblast. MDA-MB-231, U373 and 3T3-L1 were cultured in Dulbecco's Modified Eagle Medium (DMEM) with phenol red, supplemented with 10% fetal bovine serum (FBS) and 1% penicillin/streptomycin. Specifically, for LN-18 cells, the percentage of FBS was adjusted to 5%. Cell cultures were maintained at 37 °C in a humidified incubator with 5% CO_2 atmosphere until the desired confluence was achieved.

2.2.2 Determination of cell viability 3-[4,5-dimethylthiazole-2-yl]-2,5-diphenyltetrazolium bromide (MTT) assay. In brief, cells were seeded in a 96-well plate at a density of 1×10^4 cells per well. After 48 h of incubation, the cell lines were treated with **F2S4-*p*-VPA**, **F3S4-*m*-VPA** and **MTX** (positive control), at concentrations ranging from 0 μM to 300 μM for 48 h. All chemical compounds were dissolved in 0.4% DMSO, this concentration has been reported to be non-toxic for cells.[40,41]

After, 48 h of treatment, cell viability was determined by MTT assay. Firstly, the culture medium was removed, and then 20 μL of MTT solution (0.5 mg mL^{-1}) was added to each well. The cultures were then incubated for 4 h at 37 °C. After incubation, the MTT solution was removed, and the formazan salts were dissolved with 100 μL of DMSO. The absorbance was measured at 550 nm using a Multiskan EX Thermo Scientific spectrophotometer.

2.2.3 Cell migration assay. Corning Costar® TC-Treated Multiple Well Plates with 24 wells were utilized to assess cell migration capability. A total of 3×10^5 cells were seeded for MDA-MB-231 and LN-18 cell lines while 2×10^5 cells were seeded for the U373 cell line. After 24 h of incubation under the same conditions as described in the cell line and culture section, a straight line was drawn in the center of each well using a 100 μL pipette tip. The medium with residual cells was removed, and each well was washed with 300 μL of PBS. MDA-MB-231, LN-18 and U373 cells were incubated with LPS at 10 μg mL^{-1} or with LPS plus **F2S4-*p*-VPA**, **F3S4-*m*-VPA** or **MTX**. Two concentrations of each compound were evaluated 187 μM and 225 μM exposed for 48 h (near to the IC_{50} values obtained). Cell migration was observed using an inverted microscope (Motic AE20) with an AmScope MD35 microscope eyepiece camera, capturing all fields of vision.

2.2.4 Image processing. To calculate the wound areas in the cell migration assay, an online open-access software application ImageJ Version 1.53 was employed.[42] Briefly, a calibration process was conducted by measuring the scale fifty times using the same microscopy setup and capturing images with the same camera. Subsequently, the open and closed areas of each well were measured to compare the inhibitory capability of cell

migration with each compound. The percentage of wound-healing was determined using the following formula:

$$\%\ \text{Wound-healing} = 100\left(\frac{\text{initial area} - \text{trated area}}{\text{initial area}}\right)$$

2.2.5 Effect of F2S4-*p*-VPA, F3S4-*m*-VPA and MTX on apoptosis cell in MDA-MB-231 and LN-18 cell lines (anexin V-FITC/PI apoptosis assay). MDA-MB-231 and LN-18 cell lines were seeded into twelve-well plates at a density of 5×10^5 cells per well. After 24 h, the medium was replaced with DMEM with DMSO (control), as well as the compounds **F2S4-*p*-VPA**, **F3S4-*m*-VPA** and **MTX**, each at a concentration of 112 μM for LN-18 and 142 μM for MDA-MB-231. It is noteworthy that these concentrations correspond to the IC_{50} values of **F2S4-*p*-VPA**. After 48 h of treatment, medium was collected, and cells were detached with a PBS–trypsin–EDTA solution and subsequently collected by centrifugation at 4 °C and relative centrifugal force (RFC 252) *g* for 5 min. Then, cells were washed twice with PBS and centrifuged at same conditions. After discarding PBS, 300 μL of 1× binding buffer was added to suspend cells. Subsequently, 5 μL of Annexin V-FITC and 2 μL of PI were added to 100 μL of this solution and gently mixed. The mixture was then allowed to react at rt in the dark for 15 min. Finally, the samples were analyzed using a BD FACSAria™ Fusion Flow Cytometer (BD 400, USA, Becton Dickinson, BD Bioscience Inc.) equipped with FACSDiva™ v.8.0.2 acquisition and analysis software (Microsoft Windows® 10, USA, BD Biosciences Inc.). A total of 10 000 events were analyzed within the total cellular region in the FSC *vs.* SSC dot-plot.

2.2.6. Cell cycle analysis by propidium iodide (PI) staining using flow cytometry. The cell cycle phases were determined using LN-18 and 3T3-L1 cell line cultured under the conditions mentioned before until a confluence of 80% was reached. Then, the cells were synchronized using DMEM without SFB for 24 h, after 2.5×10^5 cells were seeded per well in a twelve-well plate. After 24 h, the medium was withdrawal and the treatment was added: DMEM with DMSO (control), **F2S4-*p*-VPA** and **MTX** each at a concentration of 112 μM, that corresponds to the IC_{50} value of **F2S4-*p*-VPA**. After 48 h the medium was retrieved, and cells were detached with a PBS–trypsin–EDTA solution and subsequently collected by centrifugation at 252*g* for 5 min at 4 °C. Then, the cells were washed with PBS and fixed with ethanol (70%, −20 °C), 24 h later all samples were permeabilized using permeabilization buffer (192 parts of 0.2 M Na_2HPO_4 and 8 parts of 0.1 M citric acid) for 15 min at room temperature, then were washed with PBS and added 250 μL of PBS/25 μL of pancreatic RNase (2 mg mL^{-1}) and incubated at 37 °C for 1 h. Subsequently, the samples were stained with 3 μL of PI (50 mg mL^{-1}) for 30 min at 4 °C and finally analyzed using a MACSQuant® Analyzer 16 Flow Cytometer (Miltenyi Biotec); the MACSQuantify™ and FlowJo v10 software were used for acquisition and analysis respectively. A total of 5000 events were analyzed within the total cellular region in the FSC *vs.* SSC dot-plot.

2.2.7 Determination of BAX and BCL2 protein by flow cytometric analysis. LN-18 cell line was seeded into a twelve-well-plate at a density of 2.5×10^5 cells per well, 24 h later, the medium was replaced with DMEM with DMSO (control), **F2S4-*p*-VPA** compound and **MTX** each at **F2S4-*p*-VPA** value concentration (112 μM) for 48 h. Then, the medium was collected, and cells were detached with a PBS–trypsin–EDTA solution and collected by centrifugation at 252*g* for 5 min at 4 °C. Subsequently the samples were washed with PBS, fixed with ethanol (70%, −20 °C) for 20 min and washed with PBS, they were permeabilized with permeabilization buffer (tris 0.1%) for 10 min at room temperature. After washing with PBS the anti Bax-PE (SC-7480 PE) and anti BCL-2-AF-647 (SC-7382 AF647) were added and incubated for 30 min at room temperature, finally they were washed, centrifugated and fixed using para-formaldehyde (1%). The analysis was made using a MACSQuant® Analyzer 16 Flow Cytometer (Miltenyi Biotec); the MACSQuantify™ and FlowJo v10 software were used for acquisition and analysis respectively. A total of 5000 events were analyzed within the total cellular region in the FSC *vs.* SSC dot-plot.

2.3 ADMET and physicochemical properties by AdmetSar and DataWarrior

The absorption, distribution, metabolism, excretion and toxicity (ADMET) properties of the compounds (Fig. 1) were investigated using AdmetSar (version 2.0) online software and OSIRIS DataWarrior (version 5.0) PC-version software. Initially, the SMILES notations were input into AdmetSar, which utilized machine learning to predict absorption, distribution, metabolism, excretion, and toxicity properties. Simultaneously, OSIRIS DataWarrior enabled the drawing of chemical structures, facilitating the calculation of various physicochemical properties and toxicity predictions. Results from both platforms were cross-referenced to ensure robustness. This integrated approach enhances the reliability of predicted ADMET parameters, providing a comprehensive understanding of the compounds' pharmacokinetic behaviors.

2.4 Statistical analysis

All results are presented as the mean ± SE. Statistical analyses were conducted using GraphPad Prism Version 5.00 software. One-way ANOVA was utilized for cell viability and apoptosis assays, with Dunnett's multiple comparison tests performed to analyse the wound-healing data, apoptosis assay. Statistical significance was defined as $p < 0.05$, and each experiment was repeated at least three times.

3. Results

3.1 Chemical synthesis

The characterization of **F2S4-*p*-VPA** and **F3S4-*m*-VPA** was comprehensively analyzed using IR spectroscopy, NMR, and mass spectrometry, confirming their structures and high purity. **F2S4-*p*-VPA** was characterized by IR spectroscopy, showing significant peaks at 3283 cm^{-1} for N–H stretching and 1638 cm^{-1} for C=O stretching, confirming the presence of amide and aromatic functionalities. The ^1H NMR spectrum

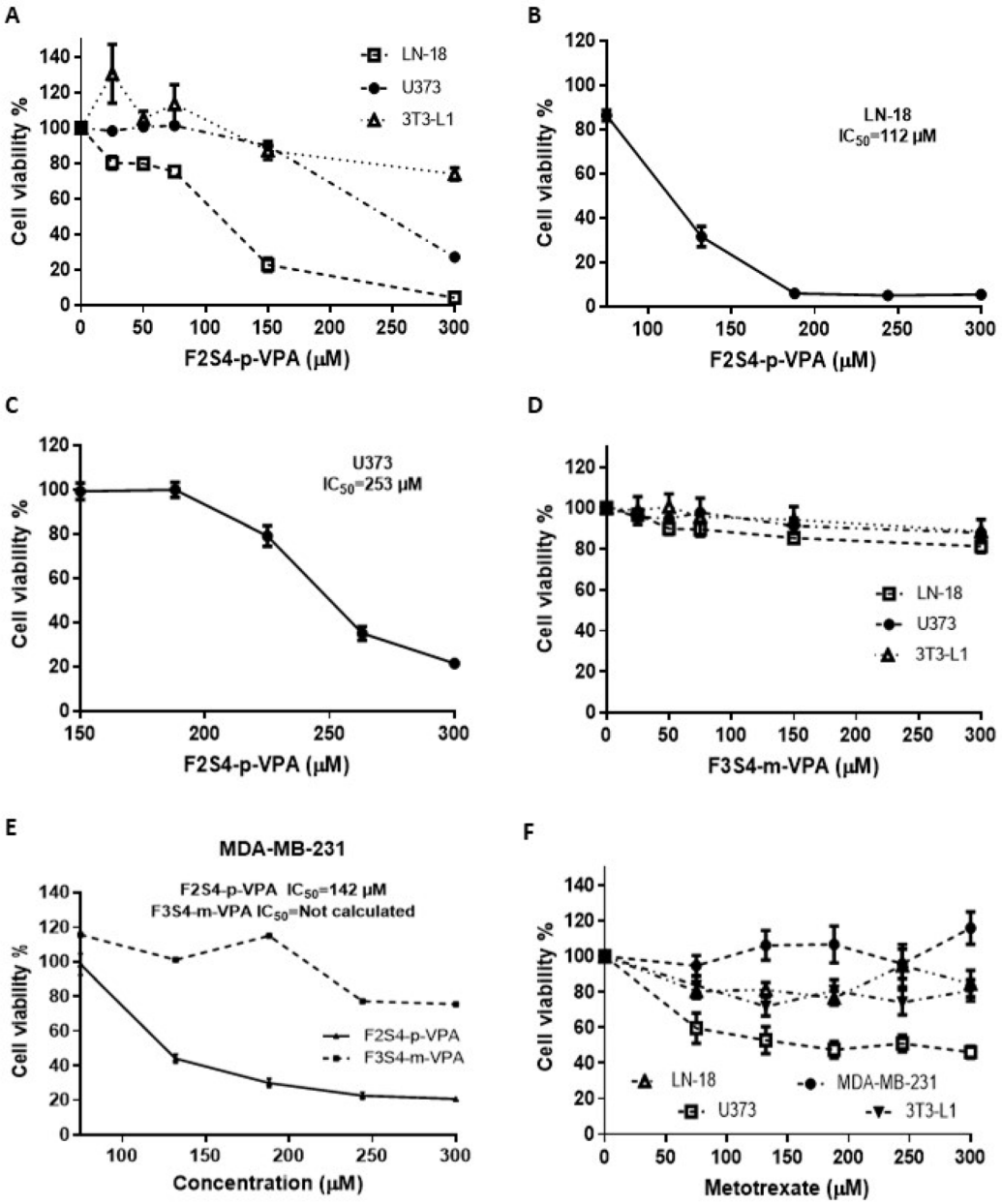

Fig. 2 Cell viability (%) after 48 h of **F2S4-*p*-VPA**, **F3S4-*m*-VPA**, and **MTX** treatment at different concentrations ranging from 0 to 300 μM in glioblastoma, breast cancer, and fibroblast cells. (A) **F2S4-*p*-VPA** on U373, LN-18 and 3T3-L1 cells lines. (B) **F2S4-*p*-VPA** on LN-18 cell line. (C) **F2S4-*p*-VPA** on U373 cell line. (D) **F3S4-*m*-VPA** on U373, LN-18 and 3T3-L1 cells lines. (E) **F2S4-*p*-VPA** and **F3S4-*m*-VPA** on MDA-MB-231 cell line. (F) **MTX** on MDA-MB-231, LN-18, U373, and 3T3-L1 cell lines. One-way ANOVA with Dunnett's multiple comparison tests was performed and results represent the mean ± the SE from three independent experiment with $n = 8$, $p < 0.05$.

revealed peaks around 6.83 ppm for aromatic hydrogens, with additional signals confirming the aliphatic chain and methoxy groups. The ^{13}C NMR spectrum featured a strong carbonyl signal at δ 175.9 ppm, along with characteristic signals for the aromatic and aliphatic regions. Mass spectrometry confirmed the molecular structure with a peak at m/z 391.2958 corresponding to the ([M] + H$^+$), the calculated molecular weight of 391.2955. The compound was obtained with a purity of 97% as determined by NMR data analysis.

Similarly, for **F3S4-*m*-VPA**, the IR spectrum displayed key absorption bands at 3290 cm^{-1} (N–H stretching), 3082 cm^{-1} (C–H stretching), 1635 cm^{-1} (C=O stretching), and 1517 cm^{-1} (aromatic C=C stretching), confirming the presence of amide, alkyl, and aromatic groups. In the ^{1}H NMR spectrum, signals were observed at 6.83 ppm for H-3 and 6.80 ppm for H-1 and H-6, consistent with aromatic protons, alongside peaks for the aliphatic chain and methoxy groups. The ^{13}C NMR showed a carbonyl signal at δ 175.9 ppm and further signals corresponding to aromatic and aliphatic carbons. Mass spectrometry provided a molecular ion peak at m/z 377.2788 ([M] + H$^+$), which closely matched the expected mass of 377.2799. The compound was isolated with a purity of 96% as determined by NMR data

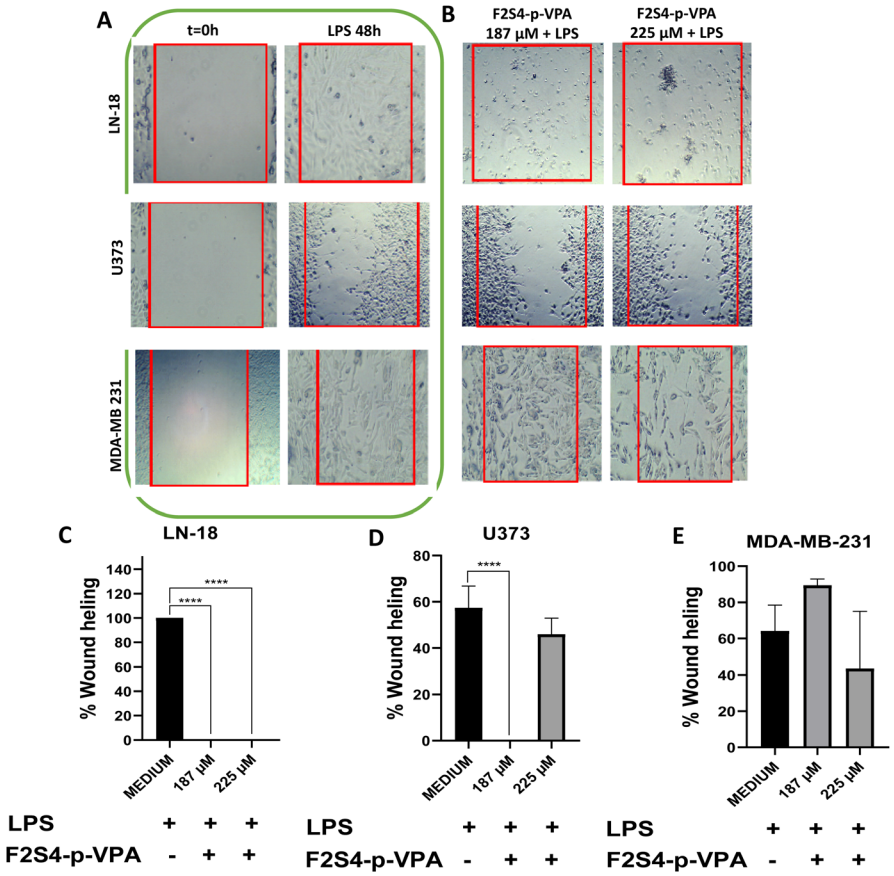

Fig. 3 LN-18, U373 and MDA-MB-231 cell lines after the treatment with LPS and F2S4-*p*-VPA. (A) Cells migration of LN-18, U373 and MDA-MB-231 cell lines after the treatment with LPS; the images are representative from three independent experiments, the images were taking at 4×. (B) Cells migration of LN-18, U373 and MDA-MB-231 cell lines after the treatment with F2S4-*p*-VPA at 185 µM + LPS and 225 µM + LPS. Percent of wound healing (C) LN-18 cells, (D) U373 cells and (E) MDA-MB-231 cells. One-way ANOVA with Dunnett's multiple comparison tests was performed and results are plotted as the mean from three independent experiments with $n = 3 \pm$ SE. ****$p < 0.0001$.

analysis. Both compounds were successfully synthesized and purified, demonstrating high yields and purity, as confirmed by the combined spectroscopic data.

3.2 Cytotoxic assays

The cytotoxic effects of **VPA** derivatives were compared with those of **MTX** by measuring the cell viability in glioblastoma cell lines (LN-18 and U373), TNBC cell line (MDA-MB-231) and a murine fibroblast cell line (3T3-L1) used this last as no cancer cells (control cells) for 48 h of treatment from 0 to 300 µM as indicated in Fig. 2.

The cell viability of U373 and LN-18 cells exposed to **F2S4-*p*-VPA** decreased in a concentration-dependent manner (Fig. 2A). Notably, **F2S4-*p*-VPA** exhibited a more pronounced cytotoxic effect on the LN-18 cell line than on the U373 cell line, with cell viability dropping to approximately 20% and 90% at 150 µM, respectively. A concentration of 300 µM of **F2S4-*p*-VPA** was required to induce significant cell death in the U373 cell line. The IC_{50} of **F2S4-*p*-VPA** against the LN-18 cell line was 112 µM (Fig. 2B) and in U373 cell line was 253 µM (Fig. 2C). Conversely, the cell viability of U373, LN-18, and 3T3-L1 cells exposed to **F3S4-*m*-VPA** from 0 to 300 µM (Fig. 2D) did not show a significant cell viability reduction.

Thus, these results showed that **F2S4-*p*-VPA** exerts a higher cytotoxic effect than **F3S4-*m*-VPA**, particularly on cancer cell lines, as evidenced by the maintenance of approximately 90% cell viability in 3T3-L1 cells at 300 µM (Fig. 2A and 2D).

The **VPA** derivatives were assayed on other aggressive cell line as TNBC (MDA-MB-231) with the same concentrations (0–300 µM) for 48 h. **F2S4-*p*-VPA** reduced cell viability with an IC_{50} of 142 µM. In contrast, **F3S4-*m*-VPA** reduced cell viability to 80% and the concentrations tested do not reach 50% (Fig. 2E).

Finally, to compare the cytotoxic effects of **MTX** across cell lines, it was incubated for 48 h at concentrations ranging from 0 to 300 µM (Fig. 2F). It was evident that **MTX** exhibited lower cytotoxicity than **F2S4-*p*-VPA**, particularly on MDA-MB-231 and 3T3-L1 cell lines. However, **MTX** exhibited a more potent cytotoxic effect on glioma cell lines, particularly on U373.

3.3 Cell migration assays

The effects of **F2S4-*p*-VPA**, **F3S4-*m*-VPA**, and **MTX** on cell migration after stimulating the cells with LPS were evaluated. Immediately after creating the wound ($t = 0$), the area was completely devoid of cells across all LN-18, U373, and MDA-MB-231 cell lines (Fig. 3A). Following 48 hours of LPS stimulation, LN-18 and MDA-MB-231 cells had covered the wound area,

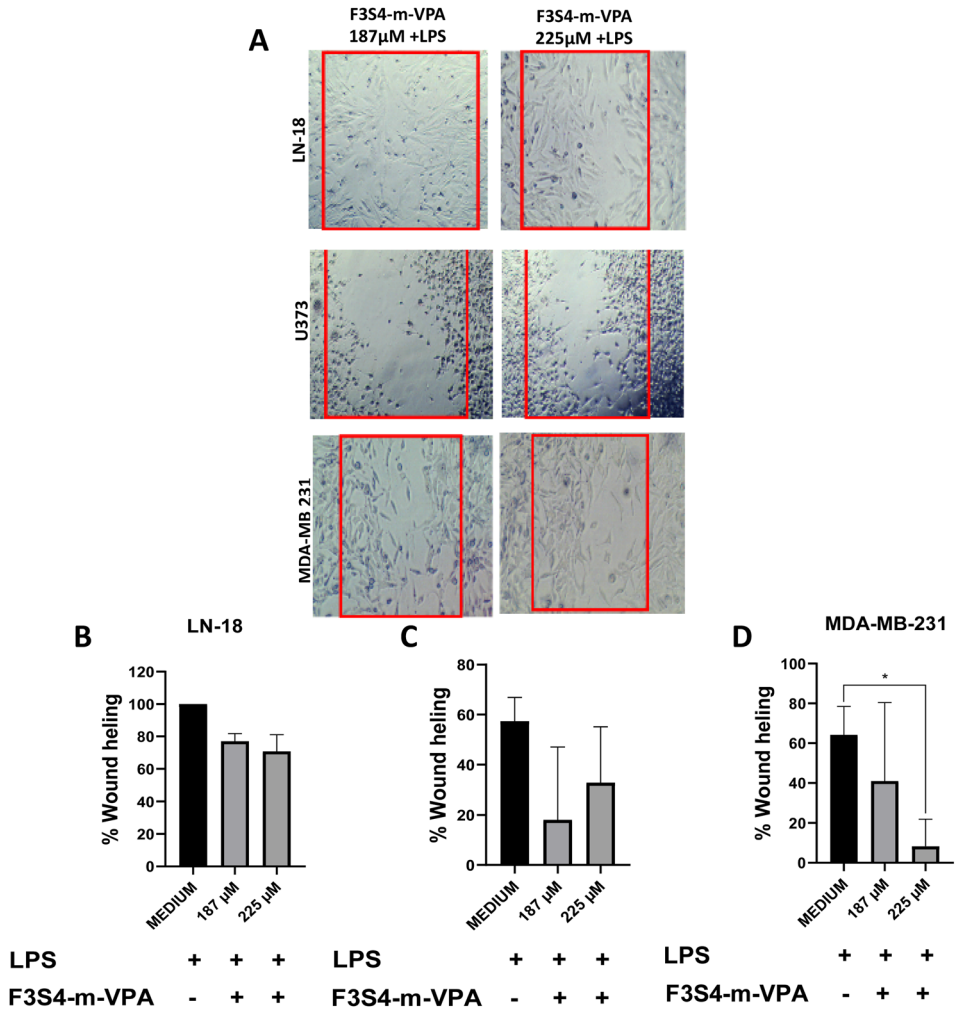

Fig. 4 LN-18, U373 and MDA-MB-231 cell lines after the treatment with F3S4-*m*-VPA and LPS. (A) Cells migration; the images are representative from three independent experiments, the images are taking at 4×. Percent of wound healing (B) LN-18 cells, (C) U373 cells and (D) MDA-MB-231 cells. One-way ANOVA with Dunnett's multiple comparison tests was performed and results are plotted as the mean from three independent experiments with $n = 3 \pm$ SE. *$p < 0.020$.

whereas U373 cells still exhibited an open wound area (Fig. 3A). Consequently, all cells were then treated with both LPS and each compound to assess whether the compounds inhibited cell migration, relative to cells treated only with LPS.

In LN-18 cells, **F2S4-*p*-VPA** at 187 μM + LPS or 225 μM + LPS resulted in minimal wound healing. The few cells remaining in the wound area exhibited an altered morphology compared to those treated solely with LPS (ESI, S9†). This suggests that at these concentrations, **F2S4-*p*-VPA** inhibits cell migration, likely due to cell death (Fig. 3B and C). Conversely, U373 cells showed higher wound healing at 225 μM, indicating that **F2S4-*p*-VPA** was more effective at inhibiting migration at 187 μM (Fig. 3D). For MDA-MB-231 cells, **F2S4-*p*-VPA** (187 μM + LPS or 225 μM + LPS) did not effectively prevent cell migration compared to the LPS-only control. Although migration decreased at 225 μM, this reduction wasn't statistically significant (Fig. 3E). Furthermore, the morphology of MDA-MB-231 cells resembled that of the LPS-only control, unlike the observations in LN-18 cells.

Treatment of LN-18 cells with **F3S4-*m*-VPA** (187 μM + LPS or 225 μM + LPS) did not effectively inhibit cell migration, with wound healing remaining around 80% (Fig. 4A and B). For U373 cells, **F3S4-*m*-VPA** demonstrated greater efficacy in preventing cell migration at 187 μM + LPS than at 225 μM (Fig. 4A); however, this difference was not statistically significant (Fig. 4C). Notably, in MDA-MB-231 cells, **F3S4-*m*-VPA** at 225 μM significantly prevented cell migration compared to the LPS control ($p < 0.020$) (Fig. 4D).

Our final evaluation focused on the effect of **MTX** across LN-18, U373, and MDA-MB-231 cell lines (Fig. 5A). In LN-18 cells, treatments with **MTX** at 187 μM + LPS or 225 μM + LPS resulted in approximately 80% wound healing. Despite this high percentage, a significant reduction in migration was observed compared to cells treated solely with LPS, suggesting a modest inhibitory effect (Fig. 5B). In contrast, U373 cells exhibited no significant differences with any **MTX** treatment, indicating a lack of migratory inhibition (Fig. 5C). For MDA-MB-231 cells, **MTX** at 225 μM was more effective in reducing wound healing

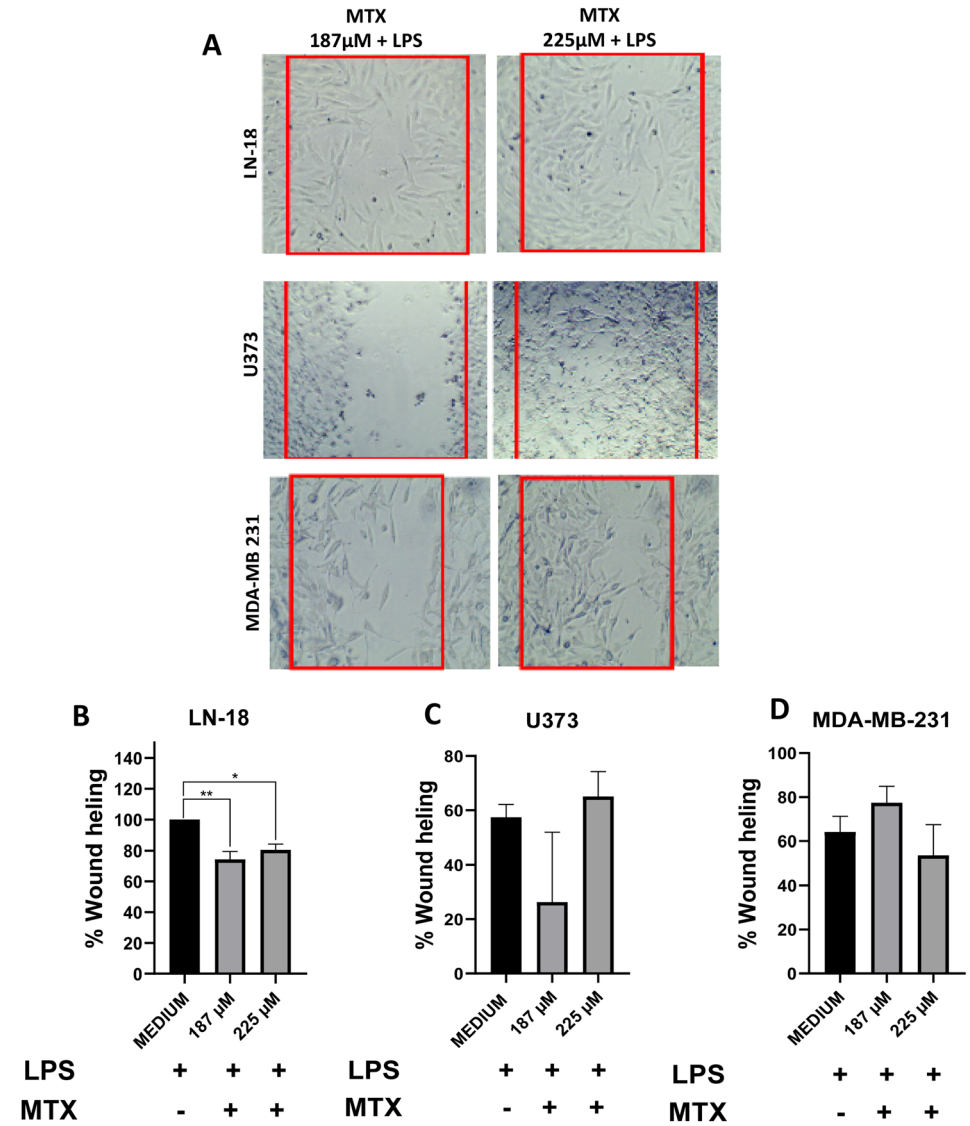

Fig. 5 LN-18, U373 and MDA-MB-231 cell lines after the treatment with MTX and LPS. (A) Cells migration of LN-18, U373 and MDA-MB-231 cell lines after the treatment with LPS; the images are representative from three independent experiments, the images are taking at 4×. Percent of wound healing (B) LN-18 cells, (C) U373 cells and (D) MDA-MB-231 cells. One-way ANOVA with Dunnett's multiple comparison tests was performed and results are plotted as the mean from three independent experiments with $n = 3 \pm$ SE. *$p < 0.020$, **$p < 0.0010$.

than at 187 μM (Fig. 5D). Therefore, **MTX** demonstrated a capacity to prevent cell migration in LPS-stimulated LN-18 cells but failed to do so in MDA-MB-231 or U373 cells.

Thus, **F2S4-*p*-VPA** demonstrated superior inhibition of LN-18 cell migration compared to **MTX**. While **F2S4-*p*-VPA** also reduced wound healing in MDA-MB-231 cells at 225 μM, its effect on cell migration was notably greater in LN-18 cells than in MDA-MB-231 cells, despite similar IC_{50} values in the cytotoxic assay.

3.4 Apoptosis assays

To determine whether the cytotoxic effect of **VPA** derivatives and **MTX** was associated with cell apoptosis, Annexin V-FITC/PI double staining was used with flow cytometry analysis. After 48 h of treatment on LN-18 cell line 6.0 ± 3.5% of cells were in the early apoptotic stage in the control group, while 28 ± 11.1%, 9 ± 5% and 13 ± 3.2% were observed in the **F2S4-*p*-VPA**, **F3S4-*m*-VPA** and **MTX** groups, respectively. The control group presented a late apoptosis percentage of 18 ± 6% whereas the **F2S4-*p*-VPA**, **F3S4-*m*-VPA** and **MTX** groups exhibited late apoptosis percentage of 15 ± 7%, 19 ± 4%, 25 ± 2%, respectively (Fig. 6A). The total percentage of late and early apoptosis caused by **F2S4-*p*-VPA** and **F3S4-*m*-VPA** were 43 ± 9% and 28 ± 5% respectively. This indicates that **F2S4-*p*-VPA** is capable of inducing apoptosis.

In the MDA MB-231 cell line, only 5.6 ± 1.7% early apoptotic cells were detected in the control group, while 8.7 ± 0.7%, 21 ± 2.3% and 12 ± 8.1% apoptotic cells were identified in the presence of **F2S4-*p*-VPA**, **F3S4-*m*-VPA** and **MTX** groups, respectively (Fig. 6B). The total percentage of late and early apoptosis caused by **F2S4-*p*-VPA** and **F3S4-*m*-VPA** were 25 ± 0.8% and 27 ± 1.4% respectively. Thus, it was observed that **F2S4-*p*-VPA**

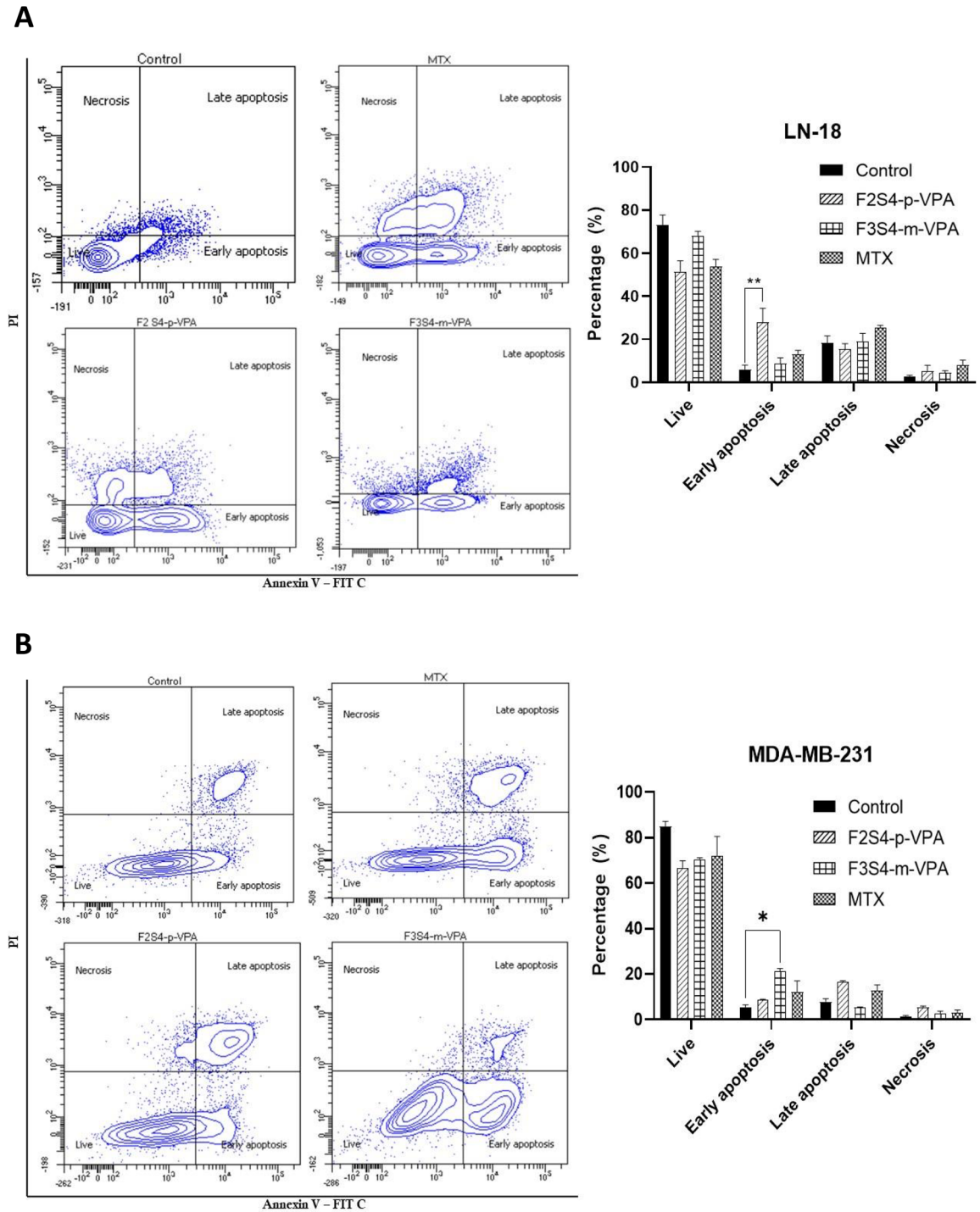

Fig. 6 Effects of **F2S4-*p*-VPA**, **F3S4-*m*-VPA** and **MTX** compounds on LN-18 and MDA-MB-231 cell lines. (A) LN-18, (B) MDA-MB-231 cells; both treated with compounds at 48 h and stained with Annexin V-FITC/PI. Statistical analysis of live, early, and late apoptosis and necrosis ratio of LN-18 and MDA-MB-231 cells after treatment was by one-way ANOVA with Dunnett's multiple comparison tests and all data are expressed as mean ± SE of three independent experiments with $n = 3$. *$p < 0.0250$, **$p < 0.0042$ compared to the control.

induces a higher proportion of cells into late apoptosis, whereas **F3S4-*m*-VPA** induces more early apoptosis. This suggests that **F2S4-*p*-VPA** is more cytotoxic, leading to apoptotic cell death rather than necrosis, as the percentage of late apoptosis is lower in all cases. Then, LN-18 cells, is more sensitive for both compounds than MDA MB-231.

3.5 Cell cycle analysis by propidium iodide (PI) staining using flow cytometry

The cells cycle phases were determinate for LN-18 and 3T3-L1 as is showed in the Fig. 7. Cell cycle analysis by flow cytometry in 3T3-L1 cell line revealed slight differences between cells treated

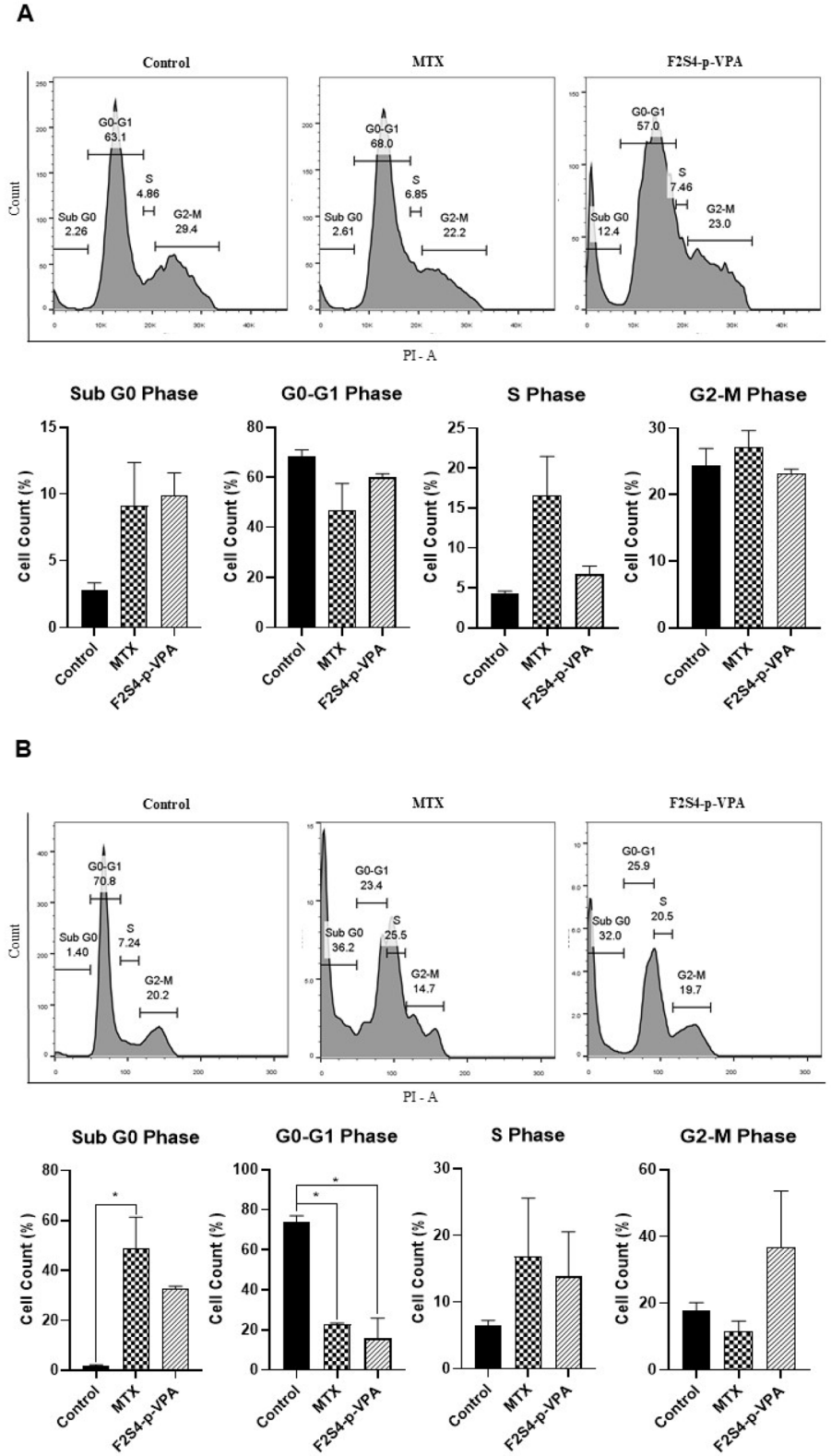

Fig. 7 Cell Cycle assay in (A) 3T3-L1 and (B) LN-18 cells. The cells were treated with medium-DMSO (control) and with **MTX** or **F2S4-*p*-VPA**. The cell cycle phases were determinate 48 h after to be treated with the compounds employing propidium iodide (PI) staining using flow cytometry. The results are from three independent experiment and the statistical analysis was by one-way ANOVA with Dunnett's multiple comparison tests and all data are expressed as mean ± SEM of three independent experiments with $n = 3$. *$p < 0.050$, compared to the control.

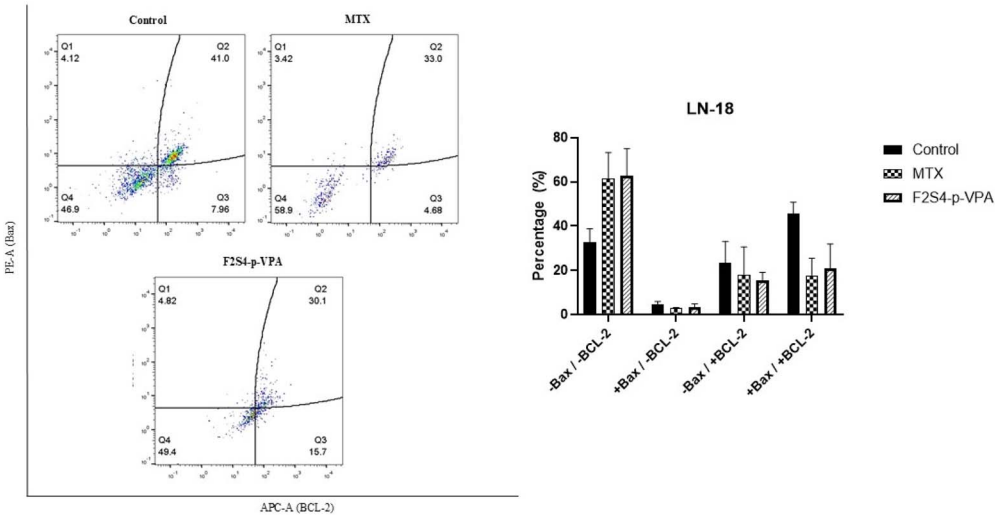

Fig. 8 Determination of BAX and BCL-2 protein on the LN-18 cell line treated with MTX and F2S4-*p*-VPA at 48 h. The results are from three independent experiment and the statistical analysis was by one-way ANOVA with Dunnett's multiple comparison tests and all data are expressed as mean ± SEM.

with **MTX** and **F2S4-*p*-VPA** (Fig. 7A) in relation with the control. The sub G0 phase shows that **F2S4-*p*-VPA** and **MTX** increases cell death (10.0% and 8% respectively) in relation with the control cells, however, there is no statistically significant difference were observed. In the G0–G1 phase it was higher in the control and in the cells treated with **F2S4-*p*-VPA** (59.9%) and **MTX** (46.8%), although it decreases around 15% with **MTX**. Regarding the S phase, it is observed that **MTX** presents a higher percentage (16.6%), which is consistent with its mechanism of action, blocking DNA synthesis. Similarly, treatment with **F2S4-*p*-VPA** also presents an increase of 6.7%, both in relation with the control cells however it was not statistically significant. Finally, in the G2–M phase, **MTX** and **F2S4-*p*-VPA** doesn't present a significant difference were observed compared to the control, these results indicated that **MTX** and **F2S4-*p*-VPA** doesn't produce a significant change in the 3T3-L1 cells.

On the other hand, in the sub G0 phase of the cell cycle analysis in LN-18 cells (Fig. 7B), it is observed that **MTX**, compared to the control, presents a statistically significant increase in cell death (48.7%), the same, in **F2S4-*p*-VPA** cell death also increases, however, there is no statistical difference. In the G0–G1 phase, both treatments (**MTX** and **F2S4-*p*-VPA**) decrease drastically to 22.7% and 15.7% respectively. In the S phase, **MTX** and **F2S4-*p*-VPA** shows double the percentage of cells compared to the control, being this 16.8% and 15.6% respectively, suggesting that it is in this phase where cell arrest occurs. In the G2–M phase, it is observed that **MTX** does not accumulate cells in this phase (11.4%), because the cells are dying earlier; Unlike **F2S4-*p*-VPA**, which has a percentage of 36.7% without presenting a significant difference compared to the control.

3.6 Bax and Bcl-2 quantification protein by flow cytometry analysis

Fig. 8 shows the percentages of Bax and Bcl-2 expression obtained from the LN-18 cell line after treatment with **MTX** and **F2S4-*p*-VPA**. In the case of **MTX**, there is a slight activation of Bax (2.8%), while the expression of Bcl-2 alone and co-expression with Bax both show an average percentage of 17.8%. Most of the cells (61.6%) showed no expression of either marker, suggesting that both genes are silenced, indicating cell death by the extrinsic apoptotic pathway. The **F2S4-*p*-VPA** sample also shows low Bax activation (3.4%), and the increase in Bcl-2 alone (15.3%) which could indicate a resistance response, possibly as a defense mechanism against the induced damage. The co-expression of both genes is intermediate (20.8%), and again, the highest percentage (62.7%) showed no expression of either marker.

3.7 *In silico* prediction of ADMET and physicochemical properties

The results of ADMET properties suggest that none of the synthesized compounds are likely to exhibit oral toxicity, as they are classified as III, while **MTX** is categorized as class II. Furthermore, according to ADMET predictions, the **VPA** derivatives can cross the BBB, unlike **MTX**. However, **VPA** derivatives may potentially induce bile salt export pump (BSEP) inhibition, which could lead to bile salt accumulation and liver toxicity, like **VPA**. Therefore, during their evaluation, it may be necessary to assess transaminases levels and other biomarkers as lactate dehydrogenase (LDH), to investigate whether these compounds, at the administrated doses, could induce liver damage or toxicity in other organs.[43] Nevertheless, only **VPA** and **MTX** were predicted to potentially cause hepatotoxicity, whereas **F2S4-*p*-VPA** and **F3S4-*m*-VPA** were not. Additionally, only **MTX** was predicted to induce nephrotoxicity (Table 1A).

None of the compounds are expected to induce carcinogenesis. Only **VPA** is identified as a CYP2C9 substrate, as previously reported, while the **VPA** derivatives could potentially act as substrates for CYP2D6, as well as for CYP3A4, including **MTX**.

However, none of the compounds are predicted to induce CYP inhibition. Nonetheless, they may potentially induce OATP1B1 and OATP1B3 inhibition, which could lead to drug accumulation and increased drug–drug interactions. However, they do not appear to inhibit OCT1 and OCT2, which are transporters for cationic substrates. The **VPA** derivatives and **MTX** were predicted to be substrates for P-glycoprotein, which could potentially reduce their efficacy by pumping the drug out of the cell and away from the target site, leading to drug resistance.[44] In terms of plasma protein binding, the **VPA** derivatives and **MTX** exhibited similar results, contrary to **VPA**. Also, is important to consider the subcellular localization of the compounds due subcellular organelles have different functions and microenvironments. The results obtained showed that all compounds could be localized in the mitochondria (Table 1), where the major biological function is related with energy conversion and storage of calcium ions.[45] However, this physiological process could be altered by the compounds and then allow that mitochondria release cyt *c*, allowing the pathway caspase activation producing apoptosis or well by increased the reactive oxygen species (ROS) which induce oxidative stress, destroy cellular structure and mitochondrial outer membrane permeability, and lead to apoptosis.[46,47] Therefore, the applications of *in silico* methods play key roles in the prediction of chemical subcellular localization due to their low costs and high performance.

Regarding to the Lipinski rule, the molecular weights of all compounds fall within the allowable range of 500 g mol^{-1}. The *c* log *P* values are lower than 5 for **F2S4-*p*-VPA**, **F3S4-*m*-VPA** and **VPA** aligning with Lipinski's criteria. However, **MTX** has a negative cLogP, indicating a preference for the aqueous phase, with a high percent (60–85%) of **MTX** excreted when administrated intravenously.[48] About hydrogen bond donors and acceptors only **MTX** exceeds the Lipinski rule allowance for acceptors, with 13 acceptors compared to the allowed, while the **VPA** derivatives have 5 hydrogen bond acceptors. Additionally, **MTX** exhibits a larger polar surface area compared to **VPA** and its derivatives. Concerning mutagenic, tumorigenic, reproductive effects, and irritancy, only **MTX** and **VPA** have a high probability, as indicated in Table 1B. Complete results from both platforms can be found in the ESI (Table 1S and 2S†).

Table 1 Absorption, distribution, metabolism, excretion, and toxicity (ADMET) and physicochemical properties obtained from AdmetSar and DataWarrior for F2S4-*p*-VPA, F3S4-*m*-VPA, VPA and MTX

(A) ADMET properties obtained by AdmetSar

	F2S4-*p*-VPA	**F3S4-*m*-VPA**	**VPA**	**MTX**
Acute oral toxicity (c)	III	III	III	II
Blood brain barrier	+	+	+	−
BSEP inhibitior	+	+	−	−
Hepatotoxicity	−	−	+	+
CYP2C9 substrate	−	−	+	−
CYP2D6 substrate	+	+	−	−
CYP3A4 substrate	+	+	−	+
Eye corrosion/eye irritation	−/−	−/−	+/+	−/−
Glucocorticoid receptor binding	+	−	−	−
Nephrotoxicity	−	−	−	+
OATP1B1 inhibitior/OATP1B3 inhibitior	+/+	+/+	+/+	+/+
OATP2B1 inhibitior	−	−	+	−
OCT1 inhibitior/OCT2 inhibitior	−/−	−/−	−/−	−/−
P-glycoprotein inhibitior	−	−	−	−
P-glycoprotein substrate	+	+	−	+
Plasma protein binding	0.692681	0.723911	0.960923	0.637697041
Subcellular localization	Mitochondria	Mitochondria	Mitochondria	Mitochondria

(B) Physicochemical properties obtained by DataWarrior

	F2S4-p-VP	**F3S4-*m*-VPA**	**VPA**	**MTX**
Mol weight	390.566	376.539	144.213	454.446
c log *P*	4.2558	3.9138	2.1912	−1.2285
H-acceptors	5	5	2	13
H-donors	1	1	1	5
Total surface area	333.67	319.91	129.66	333.45
Relative PSA	0.144	0.1502	0.2016	0.46409
Polar surface area	50.8	50.8	37.3	210.54
Druglikeness	2.9034	3.6092	−2.6221	−7.5894
Mutagenic/tumorigenic	None/none	None/none	None/none	None/high
Reproductive effective/irritant	None/none	Low/none	High/none	None/none

4. Discussion

Glioblastoma multiforme (GBM), a highly aggressive and malignant central nervous system cancer, is a leading cause of death globally, alongside other aggressive malignancies like triple-negative breast cancer (TNBC).[49–51] GBM is characterized by its migratory and invasive properties and classified by the World Health Organization (WHO) into grades II–IV, with GBM representing grade IV.[52,53] The urgent need for new drug options and evaluation methods for these aggressive cancers can be addressed by artificial intelligence (AI). Specifically, radiomics combined with machine learning (ML) offers a promising approach for analyzing imaging data, such as magnetic resonance imaging (MRI). While traditional image analysis is labor-intensive due to manual annotation, deep learning (DL), a subset of ML, can automate this process. DL is crucial for developing clinical evaluation models, detecting glioblastoma recurrence, and enabling tumor segmentation and feature extraction *via* algorithms like convolutional neural networks (CNNs). These advancements are vital for developing personalized therapeutic strategies.[54]

In drug design, modifying ligands to enhance their efficacy is crucial for developing improved anticancer agents. Valproic acid (**VPA**) has shown promise for treating various cancers, including glioblastoma. However, its effectiveness often requires high millimolar concentrations to significantly reduce cell viability and proliferation.[25] To overcome this limitation, our work proposes novel **VPA** derivatives, specifically **F2S4-*p*-VPA** (containing piperidine) and **F3S4-*p*-VPA** (containing pyrrolidine). These organic heterocyclic amines are known for their potential anticancer activity.[55–57] We hypothesized that linking **VPA** with these amines would yield superior antiproliferative effects, given their structural relation to existing anticancer drugs like methotrexate (**MTX**).

The evaluation of **VPA** derivatives and **MTX** on U373 and LN-18 (GBM) and MDA-MB-231 (TNBC) cell lines revealed that **F2S4-*p*-VPA** exhibited superior cytotoxic effects compared to **F3S4-*m*-VPA** and **MTX**. Notably, **F2S4-*p*-VPA** selectively reduced the viability of GBM cells while showing minimal impact on healthy 3T3-L1 fibroblasts. This enhanced antiproliferative effect on TNBC cells might stem from the overexpression of HDAC8 in TNBC, an enzyme known to be inhibited by **VPA**.[58,59] The IC_{50} values for **F2S4-*p*-VPA** (112 mM on LN-18; 142 mM on MDA-MB-231) indicate a stronger cytotoxic effect than both **MTX** and **VPA** (for comparison, **VPA**'s IC_{50} on MDA-MB-231 is 7.29 mM).[60] Furthermore, **MTX**'s efficacy against MDA-MB-231 is limited due to cellular resistance requiring high concentrations,[61,62] and its primary mode of action is cytostatic.[63] Our findings for **F2S4-*p*-VPA** align with previous reports of other piperidine-derived compounds showing μM-range IC50 values against MDA-MB-231.[64]

The effects of **VPA** derivatives and **MTX** on cell migration were compared, using LPS as an exogenous stimulus. This is particularly relevant as TNBC cells, like MDA-MB-231, express toll-like receptor 4 (TLR4), the lipopolysaccharide (LPS) is an agonist of TLR4 then it promotes tumor migration, invasion, and metastasis. LPS has been shown to increase invasion and migration in MDA-MB-231 and MCF-7 cells.[65] Furthermore, LPS upregulates the tumor-associated protein B7–H6, which is rarely found in normal tissues but is expressed in various tumor cells, including neuroblastoma and breast cancer. B7–H6 enhances glioma cell proliferation, migration, and invasion by modulating vimentin, *N*-cadherin, MMP-2, and MMP-9 expression[66,67] and can be induced by inflammatory factors like TLR, TNF-α, and IL-1β.[68] The migration assays showed that **F2S4-*p*-VPA** effectively halted the migration process even in the presence of LPS. At 187 and 225 mM of **F2S4-*p*-VPA** with LPS, the compound prevented cell migration, though its effectiveness varied depending on the cell; migration was more significantly reduced in MDA-MB-231 and LN-18 cells compared to U373 cells. These findings are important, as piperidine-containing compounds, such as piperine, are known to inhibit TNBC cell migration, suggesting that molecules with this heterocycle hold significant potential for inhibiting cancer cell migration and invasion.[69]

Differences in Annexin V-FITC/PI double staining assay were observed between the LN-18 and MDA-MB-231 cell lines treated with **VPA** derivatives and **MTX** as a positive control. The percentage of live cells in the control sample (untreated cells) was approximately 80%; however, upon addition of the compounds, it decreased, indicating cellular death. The concentration of the compounds used were around their IC_{50} values to maintain high quantities of cells. Nevertheless, the percentages obtained are consistent with those reported in other studies using MDA-MB-231 cells.[70] In MDA-MB-231 cells, changes in early and late apoptosis were observed when **VPA** derivatives were used. Apoptosis assays showed increased levels of early apoptosis with **F3S4-*m*-VPA** and increased levels of late apoptosis with **F2S4-*p*-VPA** indicating cell death *via* apoptosis. However, LN-18 cells highlighted sensitivity to **F2S4-*p*-VPA**, inducing higher levels of both early and late apoptosis compared to MDA-MB 231 cells. Although the compounds exhibit differences in early and late apoptosis, there are reports suggesting that apoptotic cells are functionally equivalent throughout the cell death process, there are not fully membrane integrity, as the signals or biomarkers induced by late apoptotic cells are as potent as those induced by early apoptotic cells.[71] Therefore, the treatments with these compounds resulted in noteworthy increases in the percentage of cells undergoing early apoptosis in both cell lines compared to the control groups. These findings are statistically significant ($p < 0.0001$) and imply that **F2S4-*p*-VPA** and **F3S4-*m*-VPA**, induce apoptosis, consistent with previous results demonstrating that piperidine and its derivatives such as 1-(2-(4-(dibenzo[*b*,*f*]thiepin-10-yl)phenoxy) ethyl)piperidine (DTPEP) increase cytochrome c and Bax and decrease bcl-2 in MDA-MB-231 and MCF-7 cells.[72] In addition, pyrrolidine derivatives have also shown anticancer properties, including spiro derivatives, *N*-substituted pyrrolidines, metal complexes, poly substituted derivatives, and coumarin derivatives of pyrrolidine. These compounds have demonstrated IC_{50} values in the μM range and have been evaluated in various cancer cells such as HCT116, PC-3, HepG2, FaDu, COS-7, A-549, Huh-7, MV, MCF-7, HT-29, SW-480, SH-SY5Y, MDA-MB-231,

K562, HL60, SK-OV-3, Hela, BGC-823, NCI–H1650, A2780, and MDA-MB-233.[73]

While piperidine derivatives are recognized as promising anticancer agents for prostate, lung, and breast cancers, their application in glioblastoma remains less explored.[72,73] To address this, we further investigated cell cycle arrest and Bax/Bcl-2 protein expression in LN-18 cells. The cell cycle analysis revealed distinct effects of **MTX** and **F2S4-*p*-VPA** on 3T3-L1 and LN-18 cells. In 3T3-L1 fibroblasts, both treatments decreased the G0-G1 population and slightly increased S and G2-M phases, suggesting continued cell cycle progression. Conversely, in LN-18 cells, **MTX** significantly increased the Sub G0 population (48.7%), indicating substantial cell death. Although **F2S4-*p*-VPA** also increased cell death, this was not statistically significant. Both treatments decreased the G0–G1 population and increase the S phase in LN-18 cells, implying a loss of G0/G1 checkpoint control. However, only **F2S4-*p*-VPA** induced G2-M accumulation (36.7%). This suggests that **F2S4-*p*-VPA** induces a cell cycle arrest mechanism, consistent with previous reports for piperidine derivatives causing S or G2/M arrest. These findings indicate that **F2S4-*p*-VPA** may promoting G2/M arrest even in p53-deficient cells, which could be highly beneficial for treating resistant tumors.[72,74]

The determination of Bax and Bcl-2 on the LN-18 cell line with **MTX** and **F2S4-*p*-VPA** did not induce a marked activation of Bax, which is consistent with the previously reported p53 mutation in this cell line, as this transcription factor directly regulates Bax expression.[75] Under **MTX**, most cells were concentrated in Q4 (−Bax/−Bcl-2), suggesting a cytotoxic response without specific activation of the intrinsic apoptotic pathway. In contrast, **F2S4-*p*-VPA** increased the proportion of cells in quadrant Q3 (−Bax/+Bcl-2), potentially reflecting the activation of cellular resistance mechanisms through Bcl-2 overexpression.[76] The control group showed a co-expression of Bax and Bcl-2, possibly reflecting a balance between pro- and anti-apoptotic signals.

These findings suggest that the intrinsic apoptotic pathway is not the primary mechanism of cell death induced by our treatments, implying the involvement of other pathways, such as the extrinsic route. This contrasts with Zhang *et al.*'s findings, who observed that taxol treatment in LN-18 cells increased Bax and decreased Bcl-2 expression, favoring mitochondrial pathway-mediated apoptosis.[77] Then, as was previously mentioned that the compound **F2S4-*p*-VPA** could induce apoptosis through of others Bax-independent pathways including the extrinsic pathway of apoptosis, (Fas/TNF-α/TRAIL)NoDISC → caspasa-8 → caspasa-3) then other assays are need to identify the mechanism by which **F2S4-*p*-VPA** induced apoptosis.[78] While **MTX** has been reported to alter Bax/Bcl-2 levels (increasing Bax, decreasing Bcl-2) in human hepatocyte (CRL-11233) cells,[79] specific information on its effects in LN-18 cells is scarce. Therefore, future studies investigating **F2S4-*p*-VPA**'s mechanism of cell death in cancer cells with varying p53 statuses (mutated *vs.* wild-type) would significantly enhance our understanding of its cellular mechanisms.

The prediction of ADMET properties suggests that **VPA** derivatives may exhibit hepatotoxicity. However, further evaluation *in vivo* is necessary to confirm this, as different information is obtained from two software programs (AdmetSar and DataWarrior; see ESI†). Moreover, the prediction indicates that **VPA** derivatives might be capable of crossing the BBB, which is promising for glioblastoma treatment. Considering the Lipinski rule, the **VPA** derivatives demonstrate better physicochemical behaviour than **MTX**. This is because **MTX** has a negative cLogP indicating a preference for hydrophilic media and potential elimination from the body. Additionally, **MTX** has a higher number of H-acceptors and H-donors compared to **VPA** derivatives. The subcellular localization of **MTX**, **VPA**, **F2S4-*p*-VPA** and **F3S4-*m*-VPA** was predicted by *in silico* analyses in the mitochondria, despite that the subcellular distribution can be determinate by experimental methods employing fluorescence microscopy or histochemistry among other, these are expensive and require equipment and special methodologies.[45] Then, employs *in silico* prediction of chemical subcellular localization would be practicable and helpful for molecular design and reduction of potential toxicity, due to *in silico* methods take in consideration the physicochemical properties of the molecules which are related with their chemical structures.[80,81] Ultimately, after confirming the efficacy of synthesized molecules, experimental determination of subcellular localization and ADMET properties can definitively validate these predictions.

In conclusion, our findings suggest that piperidine and **VPA**-derived compounds, particularly **F2S4-*p*-VPA**, represent promising candidates for cancer treatment, including for p53-mutated cancers. Given that **F2S4-*p*-VPA** combines two important pharmacophores (piperidine and **VPA**), further investigations into its therapeutic potential are warranted.

5. Conclusion

The present study aimed to investigate the potential activity of newly designed **VPA** derivatives, which exhibit better physicochemical and ADMET properties than **MTX** and **VPA**. Among these compounds, **F2S4-*p*-VPA** demonstrated the most potent cytotoxic effect and effectively inhibited cell migration. Therefore, **F2S4-*p*-VPA** holds promise as a potential treatment for GBM, especially considering its predicted capability to cross the blood-brain barrier. However, further research is warranted to elucidate the mechanism of action of **F2S4-*p*-VPA**.

Glossary

Glioblastoma: an aggressive type of brain cancer. Triple-negative breast cancer (TNBC): a subtype of breast cancer that lacks estrogen, progesterone, and HER2 receptors. Methotrexate (**MTX**): a common chemotherapeutic agent with low water solubility and cytostatic effects. Valproic acid (**VPA**): a chemotherapeutic agent with low potency, used to limit tumor cell proliferation. ADMET: an acronym for absorption, distribution, metabolism, excretion, and toxicity. MTT assay: a colorimetric assay for assessing cell metabolic activity, often

used to measure cell proliferation and cytotoxicity. Annexin V-FITC/PI apoptosis assay: a method to detect apoptotic cells by using Annexin V conjugated to FITC (fluorescein isothiocyanate) and propidium iodide (PI) staining. One-way ANOVA (analysis of variance): a statistical method used to compare the means of three or more samples to determine if at least one sample mean is significantly different from the others. Dunnett's multiple comparison test: a statistical test used to compare multiple treatment groups to a single control group. Wound-healing assay: an *in vitro* test to study cell migration and the effects of treatments on cell movement. ESI (Electrospray Ionization): a technique used in mass spectrometry to produce ions. Q-TOF (Quadrupole Time-of-Flight): A type of mass spectrometer that combines a quadrupole mass analyzer with a time-of-flight mass analyzer.

Abbreviations

TNBC	Glioblastoma and triple-negative breast cancer
VPA	Valproic acid
HER2	Human epidermal growth factor-2
GBM	Glioblastoma multiforme
LPS	lipopolysaccharide
PMA	Phorbol 12-myristate 13-acetate
MTX	Methotrexate
HDACIs	Histone deacetylase inhibitors
U373	Human glioblastoma astrocytoma
MDA-MB-231	Invasive ductal carcinoma
EGF	Epidermal growth factor
TGF-α	Transforming growth factor alpha
LN-18	Human malignant glioma
3T3-L1	Murine preadipocyte cell line

Data availability

If additional ESI† is required, interested parties can obtain it by contacting the first author. Requests should be directed to the following email address: marcrh2002@yahoo.com.mx. Please include specific details about the material you need and any relevant context to ensure a prompt and accurate response.

Author contributions

Conceptualization, data curation, formal analysis, supervision, investigation, writing-original draft, resources, methodology, project administration, funding acquisition, writing-review, and editing. M. C. R. H. conceptualization, data curation, formal analysis, supervision, writing-original draft. R. H. C. L. investigation, data curation, writing-review, and editing. M. O. V. methodology, investigation, data curation, formal analysis. L. G. F. M. investigation, methodology, writing-original draft. I. I. P. M. formal analysis, supervision. M. T. R. supervision, investigation. M. G. V. methodology, investigation, formal analysis, supervision. R. F. M. methodology, formal analysis, supervision J. C. B. conceptualization, funding acquisition, resources, writing-review.

Conflicts of interest

The authors of this research have no known competing financial interests or personal relationships that could appear to influence the work reported in this paper.

Acknowledgements

This work was supported by a project grant from CONAHCYT Ciencia Básica y/o de Frontera: Paradigmas y controversias de la ciencia [2022, 319355]; SIP-IPN multidiciplinario [20240059, 2297–2024]. The authors acknowledge Oscar Aurelio Martínez Romero and Alejandra Yoselín González Muñiz for their support in this research.

References

1 WHO report on cancer: setting priorities, investing wisely and providing care for all, **https://www.who.int/publications-detail-redirect/9789240001299**, Accessed March 26, 2025.
2 H. Sung, J. Ferlay, R. L. Siegel, M. Laversanne, I. Soerjomataram, A. Jemal and F. Bray, *Ca-Cancer J. Clin.*, 2021, **71**, 209–249.
3 Cancer Today, **http://gco.iarc.fr/today/home**, Accessed March 26, 2025.
4 Instituto Nacional de Estadística y Geografía, Estadísticas a propósito del día Mundial contra el Cáncer 2021, **https://www.inegi.org.mx/app/saladeprensa/noticia.html?id=6338**, Accessed March 26, 2022.
5 J. Q. Beltrán, J. E. Soto-Abraham, J. Vidaurreta-Serrano, L. G. C. Macias, E. G. Apo and E. Ogando-Rivas, *J. Neurosci. Rural Pract.*, 2018, **9**, 516–521.
6 A. D'Alessio, G. Proietti, G. Sica and B. M. Scicchitano, *Cancers*, 2019, **11**, 469.
7 G. Chandrika, K. Natesh, D. Ranade, A. Chugh and P. Shastry, *Sci. Rep.*, 2016, **6**, 22455.
8 L. Gómez-Caudillo, A. J. Ortega-Lozano, Á. G. Martínez-Batallar, H. Rosas-Vargas, F. Minauro-Sanmiguel and S. Encarnación-Guevara, *Oncol. Rep.*, 2020, **44**, 661–673.
9 G. I. Uscanga-Perales, S. K. Santuario-Facio, C. N. Sanchez-Dominguez, S. Cardona-Huerta, G. E. Muñoz-Maldonado, P. Ruiz-Flores, J. R. Barcenas-Walls, L. E. Osuna-Rosales, A. Rojas-Martinez, J. F. Gonzalez-Guerrero, J. Valero-Gomez, G. S. Gomez-Macias, A. Barbosa-Quintana, O. Barboza-Quintana, R. Garza-Guajardo and R. Ortiz-Lopez, *Oncol. Lett.*, 2019, **17**, 3581–3588.
10 M. T. Arceo-Martínez, J. E. López-Meza, A. Ochoa-Zarzosa and Z. Palomera-Sanchez, *Gac. Mex. Oncol.*, 2021, **20**, 101–110.
11 X. Li, J. Yang, L. Peng, A. A. Sahin, L. Huo, K. C. Ward, R. O'Regan, M. A. Torres and J. L. Meisel, *Breast Cancer Res. Treat.*, 2017, **161**, 279–287.
12 S. Valastyan and R. A. Weinberg, *Cell*, 2011, **147**, 275–292.
13 F. Arvelo, F. Sojo and C. Cotte, *E Cancer Med. Sci.*, 2016, **10**, 617.

14 N. M. Novikov, S. Y. Zolotaryova, A. M. Gautreau and E. V. Denisov, *Br. J. Cancer*, 2021, **124**, 102–114.
15 J. Liu, P. C. Lin and B. P. Zhou, *Curr. Pharm. Des.*, 2015, **21**, 3032–3040.
16 S. Jain, P. Dash, A. P. Minz, S. Satpathi, A. G. Samal, P. K. Behera, P. S. Satpathi and S. Senapati, *The Prostate*, 2019, **79**, 168–182.
17 M. A. Seol, J. H. Park, J. H. Jeong, J. Lyu, S. Y. Han and S.-M. Oh, *Oncotarget*, 2017, **8**, 40190–40203.
18 X. Wu, S. Qian, J. Zhang, J. Feng, K. Luo, L. Sun, L. Zhao, Y. Ran, L. Sun, J. Wang and F. Xu, *Cancer Metab.*, 2021, **9**, 23.
19 S. A. A. Rizvi, Y. Shahzad, A. M. Saleh and N. Muhammad, *Oncology*, 2020, **98**, 520–527.
20 V. Yang, M. J. Gouveia, J. Santos, B. Koksch, I. Amorim, F. Gärtner and N. Vale, *RSC Med. Chem.*, 2020, **11**, 646–664.
21 C. W. Wu, H. C. Liu, Y. L. Yu, Y. T. Hung, C. W. Wei and G.-T. Yiang, *Oncol. Rep.*, 2017, **37**, 2177–2184.
22 D. V. Lopes, A. de Fraga Dias, L. F. L. Silva, J. N. Scholl, J. Sévigny, A. M. O. Battastini and F. Figueiró, *Purinergic Signalling*, 2021, **17**, 273–284.
23 F. Figueiró, C. P. de Oliveira, L. S. Bergamin, L. Rockenbach, F. B. Mendes, E. H. F. Jandrey, C. E. J. Moritz, L. F. Pettenuzzo, J. Sévigny, S. S. Guterres, A. R. Pohlmann and A. M. O. Battastini, *Purinergic Signalling*, 2016, **12**, 303–312.
24 S. A. Brodie and J. C. Brandes, *Expert Rev. Anticancer Ther.*, 2014, **14**, 1097–1100.
25 W. Han and W. Guan, *Front. Oncol.*, 2021, **11**, 687362.
26 Y. Sixto-López, J. A. Gómez-Vidal and J. Correa-Basurto, *Appl. Biochem. Biotechnol.*, 2014, **173**, 1907–1926.
27 A. Wawruszak, M. Halasa, E. Okon, W. Kukula-Koch and A. Stepulak, *Cancers*, 2021, **13**, 3409.
28 D. Valiyaveettil, M. Malik, D. M. Joseph, S. F. Ahmed, S. A. Kothwal and M. Vijayasaradhi, *South Asian J. Cancer*, 2018, **7**, 159–162.
29 P. Prasad, H. Vasquez, C. M. Das, V. Gopalakrishnan and J. E. A. Wolff, *J. Neurooncol.*, 2009, **91**, 279–286.
30 K. Gotfryd, M. Hansen, A. Kawa, U. Ellerbeck, H. Nau, V. Berezin, E. Bock and P. S. Walmod, *Basic Clin. Pharmacol. Toxicol.*, 2011, **109**, 164–174.
31 W. Ding, D. Lim, Z. Wang, Z. Cai, G. Liu, F. Zhang and Z. Feng, *DNA Repair*, 2020, **95**, 102940.
32 Z. Cai, D. Lim, B. Jia, G. Liu, W. Ding, Z. Wang, Z. Tian, J. Peng, F. Zhang, C. Dong and Z. Feng, *Radiat. Med. Protect.*, 2023, **4**, 204–213.
33 A. Contis-Montes de Oca, E. Rodarte-Valle, M. C. Rosales-Hernández, E. Abarca-Rojano, S. Rojas-Hernández, M. J. Fragoso-Vázquez, J. E. Mendieta-Wejebe, A. M. Correa-Basurto, I. Vázquez-Moctezuma and J. Correa-Basurto, *Oncotarget*, 2018, **9**, 33368–33381.
34 C. Li, H. Chen, Q. Tan, C. Xie, W. Zhan, A. Sharma, H. Shanker Sharma and Z. Zhang, *Prog. Brain Res.*, 2020, **258**, 369–379.
35 D. Thotala, R. M. Karvas, J. A. Engelbach, J. R. Garbow, A. N. Hallahan, T. A. DeWees, A. Laszlo and D. E. Hallahan, *Oncotarget*, 2015, **6**, 35004–35022.
36 S. Berendsen, E. Frijlink, J. Kroonen, W. G. M. Spliet, W. van Hecke, T. Seute, T. J. Snijders and P. A. Robe, *Neurooncol. Adv.*, 2019, **1**, 1–8.
37 M. Farooq, A. El-Faham, S. N. Khattab, A. M. Elkayal, M. F. Ibrahim, N. A. Taha, A. Baabbad, M. A. Wadaan and E. A. Hamed, *Asian Pac. J. Cancer Prev.*, 2014, **15**, 7785–7792.
38 I. D. García Marín, R. H. Camarillo López, O. A. Martínez, I. I. Padilla-Martínez, J. Correa-Basurto and M. C. Rosales-Hernández, *PLoS One*, 2022, **17**, e0269129.
39 V. Patil, J. Pal and K. Somasundaram, *Oncotarget*, 2015, **6**, 43452–43471.
40 A. Rahimian and A. Mellati, *Razavi Int. J. Med.*, 2017, **5**, e55455.
41 P. V. Dludla, B. Jack, A. Viraragavan, C. Pheiffer, R. Johnson, J. Louw and C. J. F. Muller, *Toxicol Rep*, 2018, **5**, 1014–1020.
42 ImageJ, **https://imagej.nih.gov/ij/index.html**, accessed February 23, 2022.
43 R. Rodríguez-Pérez and G. Gerebtzoff, *Artif. Intell. Life Sci.*, 2021, **1**, 100027.
44 A. J. Ii, A. H. Aa, A. H. Kb and C. H. At, *Heliyon*, 2022, **8**, e09777.
45 N. Zheng, H. N. Tsai, X. Zhang and G. R. Rosania, *Mol. Pharm.*, 2011, **8**, 1619–1628.
46 L. Yuan, C. Wang, D. Lu, X. Zhao, L. Tan and X. Chen, *Aging*, 2020, **18**, 3662–3681.
47 T. Chuwen, L. Yifan, L. Zhuoshu, Z. Ping and Z. Mingyi, *Front. Cell Dev. Biol.*, 2022, **10**, 832356.
48 J. K. Aronson, *Side Eff. Drugs Annu.*, 2014, **35**, 821–861.
49 World Health Organization, Cancer, 2022, **https://www.who.int/news-room/fact-sheets/detail/cancer**, Accessed February 21, 2022.
50 C. Hagemann, J. Anacker, S. Haas, D. Riesner, B. Schömig, R.-I. Ernestus and G. H. Vince, *BMC Res. Notes*, 2010, **3**, 293.
51 Y. Akiyama, M. Komiyama, H. Miyata, M. Yagoto, T. Ashizawa, A. Iizuka, C. Oshita, A. Kume, M. Nogami, I. Ito, R. Watanabe, T. Sugino, K. Mitsuya, N. Hayashi, Y. Nakasu and K. Yamaguchi, *Oncol. Rep.*, 2014, **31**, 1683–1690.
52 M. Akmal, N. Hasnain, A. Rehan, U. Iqbal, S. Hashmi, K. Fatima, M. Z. Farooq, F. Khosa, J. Siddiqi and M. K. Khan, *World Neurosurg.*, 2020, **136**, 270–282.
53 T. Komori, *Neurol. Med. Chir.*, 2017, **57**, 301–311.
54 P. Chen, P. Wang and B. Gao, *Sci. Prog.*, 2024, **107**, 368504231223353.
55 M. M. Abdelshaheed, I. M. Fawzy, H. I. El-Subbagh and K. M. Youssef, *Future J. Pharm. Sci.*, 2021, **7**, 188.
56 P. Goel, O. Alam, M. J. Naim, F. Nawaz, M. Iqbal and M. I. Alam, *Eur. J. Med. Chem.*, 2018, **157**, 480–502.
57 J. Ji, F. Sajjad, Q. You, D. Xing, H. Fan, A. G. K. Reddy, W. Hu and S. Dong, *Arch. Pharm.*, 2020, **353**, 2000136.
58 G. Rahmani, S. Sameri, N. Abbasi, M. Abdi and R. Najafi, *Pathol., Res. Pract.*, 2021, **220**, 153396.
59 A. Furugen, Y. Kanno, N. Ohyama, Y. Kurosawa, N. Jinno, K. Narumi, K. Iseki and M. Kobayashi, *Drug Metab. Pharmacokinet.*, 2021, **40**, 100409.

60 A. R. Estrada-Pérez, J. B. García-Vázquez, H. L. Mendoza-Figueroa, M. C. Rosales-Hernández, C. Fernández-Pomares and J. Correa-Basurto, *Int. J. Mol. Sci.*, 2023, **24**, 14543.
61 J. Raut, O. Sarkar, T. Das, S. M. Mandal, A. Chattopadhyay and P. Sahoo, *Sci. Rep.*, 2023, **13**, 21899.
62 M. Lindgren, K. Rosenthal-Aizman, K. Saar, E. Eiríksdóttir, Y. Jiang, M. Sassian, P. Östlund, M. Hällbrink and Ü. Langel, *Biochem. Pharmacol.*, 2006, **71**, 416–425.
63 R. Seigers, S. B. Schagen, W. Beerling, W. Boogerd, O. van Tellingen, F. S. A. M. van Dam, J. M. Koolhaas and B. Buwalda, *Behav. Brain Res.*, 2008, **186**, 168–175.
64 A. Arun, M. i. Ansari, P. Popli, S. Jaiswal, A. k. Mishra, A. Dwivedi, K. Hajela and R. Konwar, *Cell Proliferation*, 2018, **51**, e12501.
65 H. Yang, B. Wang, T. Wang, L. Xu, C. He, H. Wen, J. Yan, H. Su and X. Zhu, *PLoS One*, 2014, **9**, e109980.
66 H. Wang, H. Zhi, D. Ma and T. Li, *Cytokine*, 2017, **92**, 93–102.
67 X. Wang and R. A. Khalil, *Adv. Pharmacol.*, 2018, **81**, 241–330.
68 F. Che, X. Xie, L. Wang, Q. Su, F. Jia, Y. Ye, L. Zang, J. Wang, H. Li, Y. Quan, C. You, J. Yin, Z. Wang, G. Li, Y. Du and L. Wang, *Int. Immunopharmacol.*, 2018, **59**, 318–327.
69 A. L. Greenshields, C. D. Doucette, K. M. Sutton, L. Madera, H. Annan, P. B. Yaffe, A. F. Knickle, Z. Dong and D. W. Hoskin, *Cancer Lett.*, 2015, **357**, 129–140.
70 J. I. Noh, S. K. Mun, E. H. Lim, H. Kim, D. J. Chang, J. S. Hur and S. T. Yee, *J. Fungi*, 2021, **7**, 188.
71 V. A. Patel, A. Longacre, K. Hsiao, H. Fan, F. Meng, J. E. Mitchell, J. Rauch, D. S. Ucker and J. S. Levine, *J. Biol. Chem.*, 2006, **281**, 4663–4670.
72 S. Mitra, U. Anand, N. K. Jha, M. S. Shekhawat, S. C. Saha, P. Nongdam, K. R. R. Rengasamy, J. Proćków and A. Dey, *Front. Pharmacol.*, 2022, **12**, 772418.
73 A. A. Bhat, I. Singh, N. Tandon and R. Tandon, *Eur. J. Med. Chem.*, 2023, **246**, 114954.
74 V. Srivastava, M. Y. Wani, A. S. Al-Bogami and A. Ahmad, *J. Adv. Res.*, 2021, **29**, 121–135.
75 I. Wybranska, A. Polus, M. Mikolajczyk, A. Knapp, A. Sliwa, B. Zapala, T. Staszel and A. Dembinska-Kiec, *Hum. Cell*, 2013, **26**, 137–148.
76 T. J. McDonnell, A. Beham, M. Sarkiss, M. M. Andersen and P. Lo, *Cell. Mol. Life Sci.*, 1996, **52**, 1008–1017.
77 R. Zhang, N. L. Banik and S. K. Ray, *Brain Res.*, 2008, **1239**, 216–225.
78 S. Shen, Y. Shao and C. Li, *Cell Death Discovery*, 2023, **9**, 284.
79 A. G. Kabakci, H. Kaplan, E. Şingirik and M. G. Bozkır, *J. Pharm. Res. Int.*, 2021, **33**, 2227–2236.
80 H. Yang, X. Li, Y. Cai, Q. Wang, W. Li, G. Liu and Y. Tang, *Med. Chem. Commun.*, 2017, **8**, 1225–1234.
81 N. Zheng, H. N. Tsai, X. Zhang, K. Shedden and G. R. Rosania, *Mol. Pharm.*, 2011, **8**, 1611–1618.